materials

MDPI

Review

Gallium Oxide for Gas Sensor Applications: A Comprehensive Review

Jun Zhu [1], Zhihao Xu [2], Sihua Ha [3], Dongke Li [4,*], Kexiong Zhang [5], Hai Zhang [3,*] and Jijun Feng [6,*]

1 School of Physical Science and Technology, Inner Mongolia University, Hohhot 010021, China
2 Global Zero Emission Research Center (GZR), National Institute of Advanced Industrial Science and Technology (AIST), Tsukuba 3058560, Japan
3 College of Sciences, Inner Mongolia University of Technology, Hohhot 010051, China
4 ZJU-Hangzhou Global Scientific and Technological Innovation Center, School of Materials Science and Engineering, Zhejiang University, Hangzhou 311200, China
5 School of Microelectronics, Dalian University of Technology, Dalian 116602, China
6 Shanghai Key Laboratory of Modern Optical System, Engineering Research Center of Optical Instrument and System (Ministry of Education), School of Optical-Electrical and Computer Engineering, University of Shanghai for Science and Technology, Shanghai 200093, China
* Correspondence: ldkest@zju.edu.cn (D.L.); z_hai@imut.edu.cn (H.Z.); fjijun@usst.edu.cn (J.F.)

Abstract: Ga_2O_3 has emerged as a promising ultrawide bandgap semiconductor for numerous device applications owing to its excellent material properties. In this paper, we present a comprehensive review on major advances achieved over the past thirty years in the field of Ga_2O_3-based gas sensors. We begin with a brief introduction of the polymorphs and basic electric properties of Ga_2O_3. Next, we provide an overview of the typical preparation methods for the fabrication of Ga_2O_3-sensing material developed so far. Then, we will concentrate our discussion on the state-of-the-art Ga_2O_3-based gas sensor devices and put an emphasis on seven sophisticated strategies to improve their gas-sensing performance in terms of material engineering and device optimization. Finally, we give some concluding remarks and put forward some suggestions, including (i) construction of hybrid structures with two-dimensional materials and organic polymers, (ii) combination with density functional theoretical calculations and machine learning, and (iii) development of optical sensors using the characteristic optical spectra for the future development of novel Ga_2O_3-based gas sensors.

Keywords: Ga_2O_3; electric properties; preparation methods; gas sensors; enhancement strategies

Citation: Zhu, J.; Xu, Z.; Ha, S.; Li, D.; Zhang, K.; Zhang, H.; Feng, J. Gallium Oxide for Gas Sensor Applications: A Comprehensive Review. *Materials* **2022**, *15*, 7339. https://doi.org/10.3390/ma15207339

Academic Editor: Marina N. Rumyantseva

Received: 19 September 2022
Accepted: 12 October 2022
Published: 20 October 2022

1. Introduction

Gallium oxide (Ga_2O_3), as one type of ultrawide bandgap (UWBG) semiconducting material [1], has received tremendous attention ever since 2012 when Higashiwaki et al. successfully developed the first single-crystal Ga_2O_3 field-effect transistors (FETs) [2]. Over the past decade, Ga_2O_3 has found main applications in power electronics, solar-blind ultraviolet (UV) photodetectors, and radiation detectors, as well as gas sensors [3,4]. A variety of electronic and optoelectronic devices such as Schottky barrier diodes (SBDs) [5,6] and FETs, including MESFETs, MOSFETs, MODFETs, and HEMTs [6–9] based on Ga_2O_3 bulk single crystals, thin films, and nanostructured materials, have been achieved thanks to the advance in growth and characterization technologies and the unique properties of Ga_2O_3. There have been tens of review articles [5–40] concerning Ga_2O_3 that cover the growth techniques, the physical and chemical properties, and the state-of-the-art device fabrications. Although initial studies on the gas-sensing properties of Ga_2O_3 thin films were launched by Fleischer and Meixner [41,42] in the early 1990s, few review papers on Ga_2O_3-based gas sensors exist in the literature. Except for a complete review [26,27] that focuses on the gas sensors made by β-Ga_2O_3 nanowires and thin films, the related review can be only found in several works [4,14,15], which are usually not specialized in the domain of sensors.

It is known that Ga_2O_3 is a very important gas-sensing material widely used for monitoring exhaust gases of automobiles, flue gases of incinerators, pollutant gases of refinery plants, and explosive gases from military applications [43]. The exploration of Ga_2O_3-based gas sensors has never broken off in the last three decades, and more than five publications on average were present every year, as evident from Figure 1. In this article, we give a comprehensive overview on the distinctive aspects of Ga_2O_3 for gas sensor applications. The rest of the article is organized as follows. The polymorphs and crystal structures of Ga_2O_3 are presented in Section 2, followed by an introduction of the basic electrical properties of Ga_2O_3 in Section 3. The preparation methods used for fabricating Ga_2O_3-sensing material are provided in Section 4. Four key aspects in Ga_2O_3-based gas sensors, i.e., sensing mechanisms, evaluation criteria, classification of typical sensors, and performance enhancement strategies, are discussed in Section 5. Finally, a brief conclusion and outlook will be described in the last section.

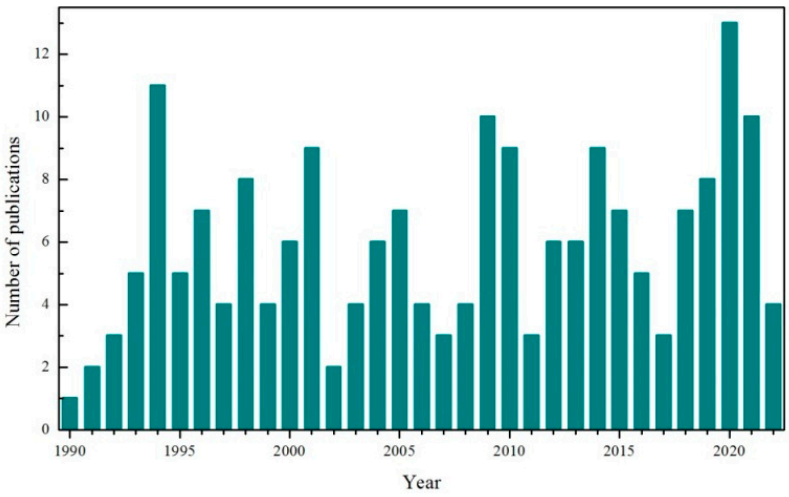

Figure 1. Number of publications on Ga_2O_3-based gas sensors from 1990 to 2022. Data extracted from Web of Science with keywords "sensor" or "sensing" and "Ga_2O_3" or "gallium oxide".

2. Polymorphs and Crystal Structures of Ga_2O_3

In the context of crystallography, polymorphism is the occurrence of different crystal structures for the same chemical entity [44]. Roy et al. [45] first identified the polymorphs of Ga_2O_3 by X-ray diffraction (XRD) when studying the phase equilibriums of the Al_2O_3-Ga_2O_3-H_2O system in 1952. They reported that there were five polymorphs of Ga_2O_3, labeled as α, β, γ, δ, and ε. The polymorphs were further confirmed by Yoshioka et al. [46] via first-principle calculations and by Zinkevich and Aldinger [47] via thermodynamic theoretical calculations. The Ga-O binary phase diagram has been also established for the first time in the work of Zinkevich and Aldinger [47]. Playford et al. [48] and Cora et al. [49] discovered the new κ-phase of Ga_2O_3 with a mixture of the β- or ε-phase. The electronic structures and polar properties of κ-Ga_2O_3 were demonstrated using density functional theory (DFT) [50]. Single-domain κ-Ga_2O_3 thin films have been successfully grown on the ε-$GaFeO_3$ substrate by Nishinaka et al. in 2020 [51]. XRD φ-scan and transmission electron microscopy (TEM) revealed that the as-grown κ-Ga_2O_3 thin films comprised a single-domain, and none of the in-plane rotational domains were present in the films.

A summary of these six polymorphs observed in Ga_2O_3 until now is presented in Table 1. Among these polymorphs, β-phase is the most stable thermodynamically. All the other polymorphs are metastable and will transform into β-phase over a certain temperature, as shown in Figure 2. The interconversion of other Ga_2O_3 polymorphs possibly occurs under different temperatures and pressures. The formation-free energies of all the phases except κ follow the $\beta < \varepsilon < \alpha < \delta < \gamma$ order at a low temperature [46]. Figure 3a depicts the schematic crystal structure of each polymorph. Almost all the phases demonstrate anisotropy. Taking β-Ga_2O_3 as an example, it is clearly seen from Figure 3b that the atomic

arrangements for each crystal plane are different, which leads to different atomic configurations and dangling bond densities and therefore nonequivalent sensing properties along different crystal orientations [52].

Table 1. Basic properties of Ga_2O_3 polymorphs [22,32].

Polymorph	System	Space Group	Lattice Parameters
α	hexagonal	$R\bar{3}c$	$a = b = 4.98–5.04$ Å, $c = 13.4–13.6$ Å, $\alpha = \beta = 90°$, $\gamma = 120°$
β	monoclinic	C2/m	$a = 12.12–12.34$ Å, $b = 3.03–3.04$ Å, $c = 5.80–5.87$ Å, $\alpha = \beta = 90°$, $\gamma = 103.8°$
γ	cubic	$Fd\bar{3}m$	$a = b = c = 8.24–8.30$ Å, $\alpha = \beta = \gamma = 90°$
δ	cubic	Ia3	$a = b = c = 9.40–10.1$ Å, $\alpha = \beta = \gamma = 90°$
ε	hexagonal	P63mc	$a = 5.06–5.12$ Å, $b = 8.69–8.79$ Å, $c = 9.3–9.4$ Å, $\alpha = \beta = 90°$, $\gamma = 120°$
κ	orthorhombic	$Pna2_1$	$a = 5.05$ Å, $b = 8.69$ Å, $c = 9.27$ Å, $\alpha = \beta = \gamma = 90°$

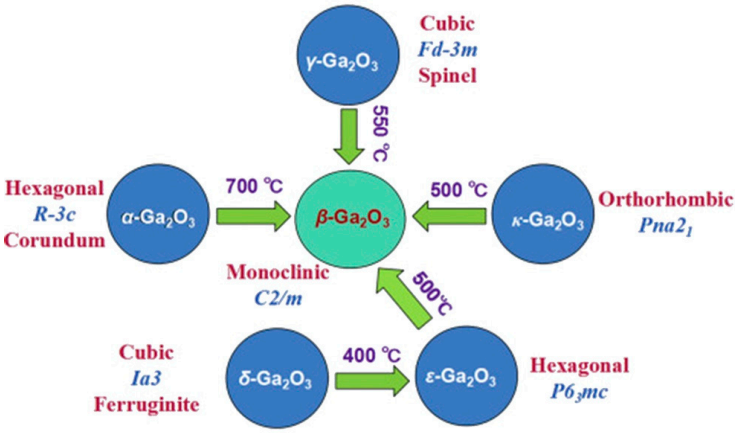

Figure 2. Interconversion relation of Ga_2O_3 polymorphs [22]. Copyright 2019 Elsevier.

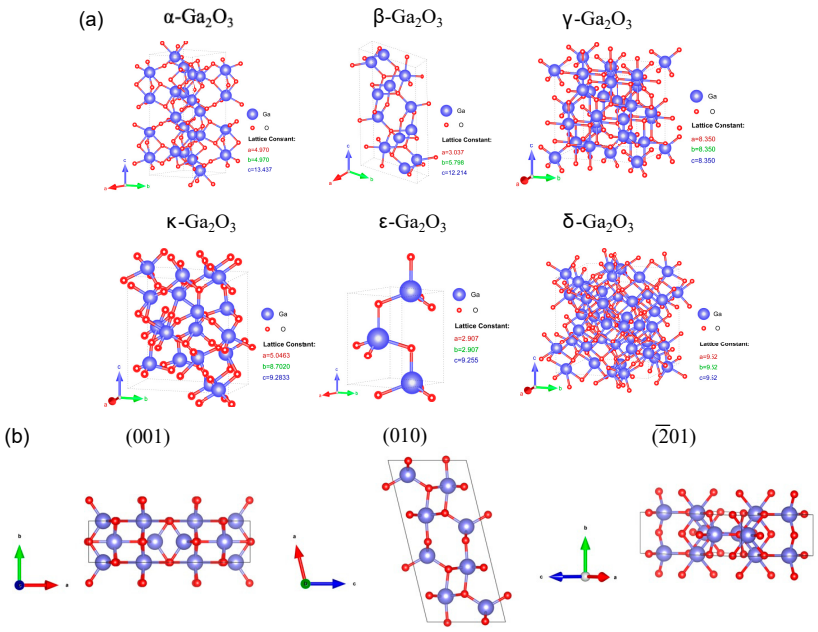

Figure 3. (**a**) Crystal structures of six polymorphs of Ga_2O_3. (**b**) The (001), (010), and ($\bar{2}$01) planes for β-Ga_2O_3. Original drawing using VESTA was done by us.

3. Electrical Properties of Ga_2O_3

It is of interest to understand the electrical properties of Ga_2O_3 that play a critical role in determining the operation and functionality of a gas sensor.

As known, the electrical conductivity (σ) of a semiconductor has a relationship with the carrier concentration (n) and carrier mobility (μ), which are written as

$$\sigma = en\mu, \quad (1)$$

where e is the elementary charge.

Theoretically, undoped stoichiometric Ga_2O_3 is a transparent insulator because of its ultrawide bandgap of ~4.9 eV. However, the as-prepared Ga_2O_3 exhibits intrinsic n-type conductivity, and the reason for the unintentional doping is still under debate. Oxygen vacancies have been considered as a source of the intrinsic electrical conductivity for a long time [53,54]. Varley et al. [55] suggested that oxygen vacancies should act as deep donors that cannot directly account for the intrinsic electrical conductivity, because the ionization energy of such vacancies was calculated as more than 1 eV. It has been widely accepted that residual impurities such as Si and H with lower formation energies in the growth process have possibly given rise to the underlying conductivity of Ga_2O_3 since then [14,15,29]. By doping impurities such as Sn, Si, and Ge in Ga_2O_3, the free electron concentration could reach the magnitude of 10^{19} cm^{-3} in the bulk crystals and 10^{20} cm^{-3} in the case of thin films at room temperature [25,28,29,37]. In general, the ionization energy of the shallow donors has a value of less than 70 meV, which decreases with the dopant concentration. For instance, the ionization energy for Sn ranges from 7.4 meV to 60 meV; for Si, ranges from 16 meV to 50 meV; and for Ge, ranges from 17.5 meV to 30 meV [29]. The free electron concentration can be also increased by the growth conditions and post-thermal treatment [15]. However, p-type doping of Ga_2O_3 is still a huge challenge.

So far, the measured room temperature Hall mobility in β-Ga_2O_3 reaches 184 cm^2/Vs [56], lower than the theoretical predicted value of 300 cm^2/Vs [2]. The electron mobility varies as functions of the temperature and carrier density. Fleischer and Meixner [57], Irmscher et al. [58], Ma et al. [59], and Gato et al. [60] studied the temperature dependence of the electron mobility of single-crystal and polycrystalline Ga_2O_3 through Hall effect measurements. As shown in Figure 4, both the electron density and the Hall mobility increase with the increasing temperature. At an elevated temperature, the electron mobility in both cases is not determined by grain boundaries but the crystal lattice itself [57]. The intrinsic mobility is limited by optical phonon scattering at a high temperature and by ionized impurity scattering at a low temperature [59]. Moreover, the electron mobility falls when the electron density increases. The electronic effective mass at low and moderate free electron concentrations is estimated at about 0.28 of the free electronic mass, and the static dielectric constant is near 10 [61]. Table 2 highlights the basic electric properties of β-Ga_2O_3 reviewed in the literature. It should be pointed out that these material parameters, including electronic mobility, electronic effective mass, and dielectric constant, are greatly modified by the crystal anisotropy effect.

Table 2. Basic electric properties of β-Ga_2O_3 [32,61].

Electric Properties	Value
Electronic effective mass (m_0)	0.28
Static dielectric constant	10
High frequency dielectric constant	3.9
Electron mobility ($cm^2 \cdot V^{-1} \cdot s^{-1}$)	200
Range of free electron concentration (cm^{-3})	10^{16}~10^{20}
Range of doping concentration (cm^{-3})	10^{17}~10^{20}
Electron affinity (eV)	4.0
Break down field (eV/cm)	8.0
Typical types of shallow donors	Sn, Ge, Si

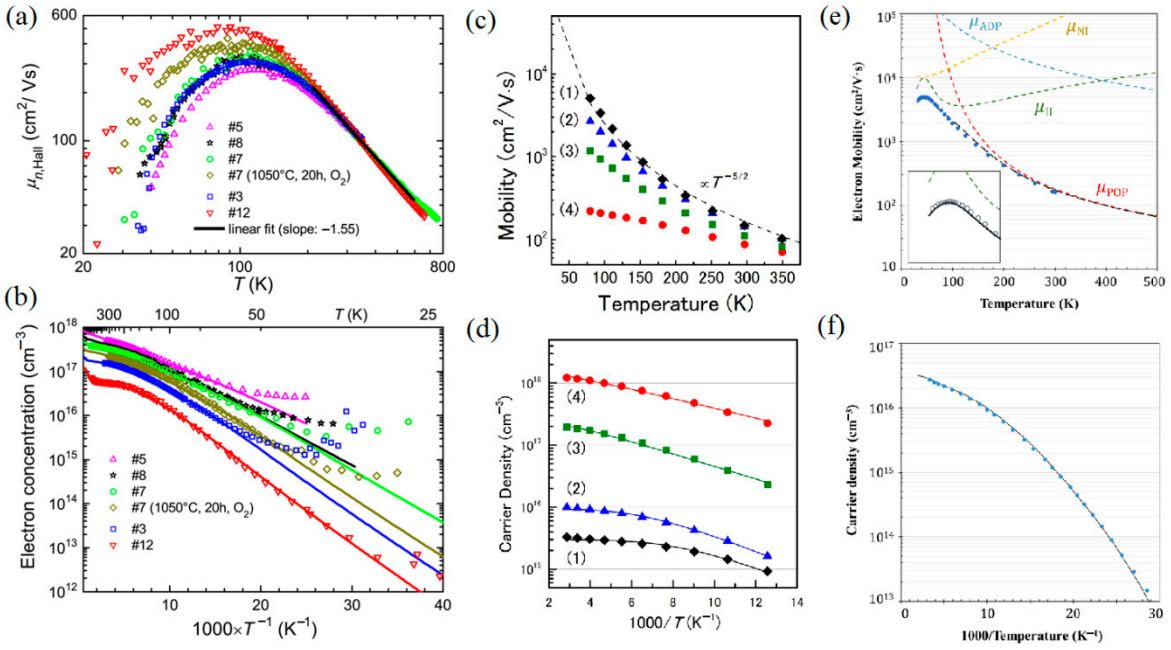

Figure 4. (**a**) The Hall mobility and (**b**) electron density as functions as the temperature for β-Ga_2O_3 single crystals grown by the Czochralski method [58]. Copyright 2011 American Institute of Physics. (**c**) The Hall mobility and (**d**) electron density as functions as the temperature for Si-doped homoepitaxial films grown on β-Ga_2O_3 (001) substrate by halide vapor-phase epitaxy [60]. Copyright 2018 Elsevier. (**e**) The Hall mobility and (**f**) electron density as functions as the temperature for silicon-doped β-Ga_2O_3 homoepitaxial films grown on β-Ga_2O_3 (010)-oriented substrates via metalorganic chemical vapor deposition [56]. Copyright 2019 American Institute of Physics.

4. Preparation Methods of Ga_2O_3 Gas-Sensing Material

Owing to its high chemical and thermal stability, Ga_2O_3 is regarded as an important n-type gas-sensing material [43]. Amidst six polymorphs, β-Ga_2O_3 is the most favorable modification for constructing gas sensors. Sometimes, the amorphous [62–64] and metastable phases [65,66] of Ga_2O_3 have also been proposed for the purposes of detecting oxygen, ozone, and so on. Nonstoichiometric amorphous film with certain degree of oxygen vacancy leads to a lower electric conductivity and, thus, a faster rising response and a higher sensitivity to O_2 [62,63]. The amorphous Ga_2O_3 thin films, which were decorated with InGaZnO nanoparticles, showed a boosted room temperature-sensing capability of ozone [64]. α- and ε (κ)-Ga_2O_3 thin films demonstrated sensing properties towards a large amount of oxidizing and reducing gases [65,66]. Usually, bulk crystals; thin films; and nanostructures (e.g., nanowires, nanorods, nanoparticles, etc.) have been prepared for various types of gas sensors. In this section, particular emphasis is placed on the commonly used growth techniques to prepare Ga_2O_3-sensing material.

4.1. Bulk Single-Crystal Growth

As for gas sensor applications, a few melt growth techniques have been used for preparing bulk β-Ga_2O_3 single crystals. These techniques contain the floating zone (FZ) [67–69], Czochralski (CZ) [70,71], and edge-defined film-fed (EFG) [52] growths. At high temperatures, β-Ga_2O_3 single crystal shows an oxygen-sensing property by the electrical resistance measurement. Oxygen diffusion in bulk takes place more likely by interstitial migration rather than by vacancy migration. The hydrogen-sensing characteristics of Pt Schottky diodes have been investigated using $(\bar{2}01)$ and (010) β-Ga_2O_3 single crystals grown by the FZ and EFG methods. Different gallium and oxygen atomic configurations of Ga_2O_3 surfaces result in somewhat distinctive hydrogen responses of $(\bar{2}01)$ and (010) facets. However, it remains unknown which is the chemical active crystal face of β-Ga_2O_3. The carrier

mobility in single-crystal and polycrystalline ceramics was shown to be identical by the high-temperature Hall measurements [57]. Therefore, Ga_2O_3 polycrystalline thin films and nanostructures have become more popular than bulk crystals for advanced gas sensors. Since there have been quite a bit of research on gas-sensing characteristics of β-Ga_2O_3 single crystals, the bulk crystal growth methods of Ga_2O_3 are not discussed in detail here and can be found in other reviews [3,14–16,36]. Numerous approaches have been employed for the preparation of Ga_2O_3-sensing materials in the form of thin film and nanostructures. Later on, we will focus our discussion on the four most prevalent synthesis routes in the literature: magnetron sputtering, chemical vapor deposition (CVD), sol–gel synthesis, and hydrothermal synthesis.

4.2. Magnetron Sputtering

One of the most popular techniques for the growth of Ga_2O_3-sensing material is magnetron sputtering because of its low cost, simplicity, and low operating temperature. It is a physical vapor deposition technique to deposit thin films in which atoms are removed from a sintered target by bombardment with positive gas ions such as Ar^+. A magnetic field is added beneath the target to create plasma at lower working pressures and to deflect and confine electrons. Since gallium has a low melting point of 29.8 °C, Ga_2O_3 thin films can be sputtered only from the metal oxide target. A radio frequency (RF) voltage is usually applied in order to prevent the target from charging up due to the bombardment from positively charged ions, as the Ga_2O_3 target is an insulating ceramic one. Saikumar et al. [24] provided a review of RF-sputtered films of Ga_2O_3 and clarified the influences on the crystallinity and film properties of Ga_2O_3 from various sputtering parameters, such as substrate temperature, sputtering power, annealing temperatures, and oxygen partial pressure in the reactive sputtering.

Different substrates such as sapphire [72–88], BeO [41,42,89–97], silicon [98–101], and quartz glass [101–104] frequently equipped with an interdigital electrode have been chosen to deposit Ga_2O_3-sensing layers using the sputtering technique. The obtained films are polycrystalline or amorphous Ga_2O_3 thin films. After post annealing, the sputtering β-Ga_2O_3 polycrystalline films are very suitable for making high-temperature sensors owing to their low-term chemical stability. Ga_2O_3 with incomplete crystallinity or the amorphous phase has also aroused interest in a room temperature ozone sensor due to the large base resistance and oxygen vacancies [64]. Figure 5 shows the AFM images and XRD patterns of the Cr-doped β-Ga_2O_3 thin films synthesized on the sapphire substrates by means of RF magnetron sputtering of the Ga_2O_3 target in oxygen–argon plasma. After annealing, the Ga_2O_3 thin films with and without the addition of Cr dopant had a β-phase polycrystalline structure, and the average grain size was estimated to be 90–100 nm for pure β-Ga_2O_3 and 25–50 nm for Cr-doped β-Ga_2O_3. However, the main drawback for gas sensor applications is that the sputtered films are too compact to increase the specific surface area.

4.3. Chemical Vapor Deposition

Chemical vapor deposition (CVD) is particularly interesting not only because it gives rise to high-quality Ga_2O_3 thin films and nanostructures but also because it is applicable to large-scale production [105]. CVD, also referred to as chemical vapor transport or vapor phase epitaxy, is a conventional method often using a multitemperature zone tubular furnace (see Figure 6a) or a stainless steel chamber as a reactor. As metal organic precursors are used, the CVD technique is called MOCVD, while, in the case of hydride or halide precursors, the technique is named HVPE. Strictly speaking, thermal oxidation should not belong to the CVD technique. It will be discussed together in this section due to the high growth temperature and chemical reaction in an activated gaseous environment similar to CVD. In the CVD process, the reactant gases are diluted in carrier gases and introduced into the reaction chamber or region. When the reactant gases approach the surface of the heated substrate, chemical reactions occur on the surface to form the deposited material. The energy necessary to start the desired chemical reaction can be supplied as thermal

energy or photon energy or glow discharge plasma. Gaseous reaction by-products are then evacuated with the carrier gas by a rotary pump.

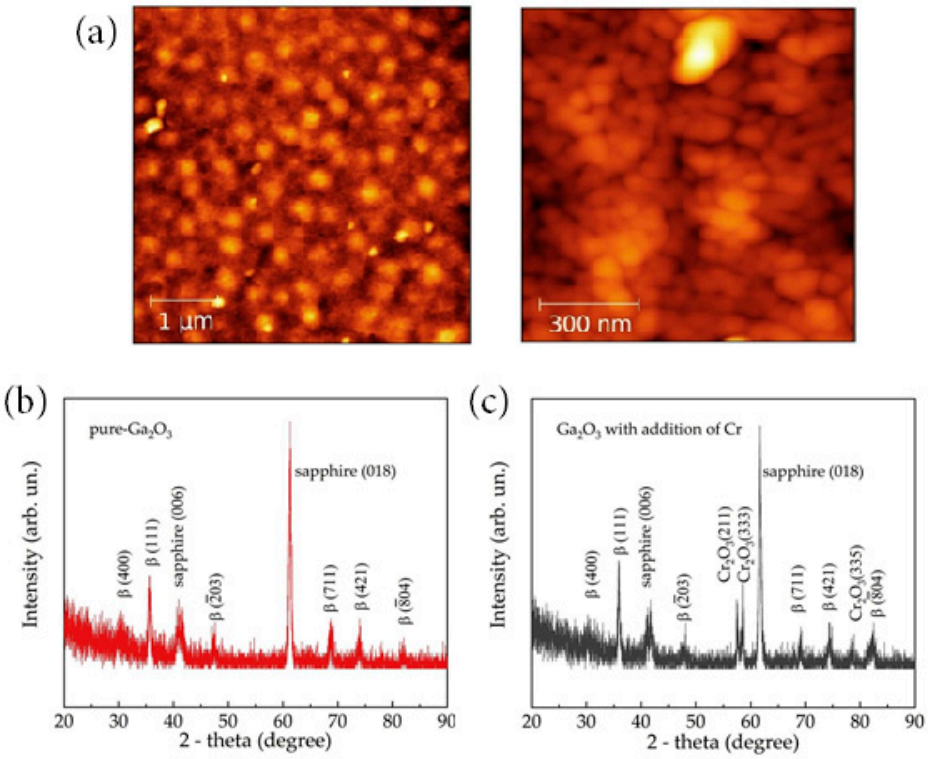

Figure 5. (**a**) AFM images of the Cr-doped Ga_2O_3 sputtering thin film [87]. XRD patterns of (**b**) pure Ga_2O_3 thin films and (**c**) Cr-doped Ga_2O_3 thin films [87]. Copyright 2020 Elsevier.

For the growth of Ga_2O_3-sensing material, liquid gallium [106–123], gallium nitride [124–132], gallium sulfides, including Ga_2S_3 [133] and GaS [134], gallium acetylacetonate [135], and gallium chloride [65,66,136–138] are often used as the gallium source, while pure oxygen or water vapor is selected as the oxygen source. Argon or nitrogen is used as the carrier gas. Sometimes, a mixture of Ga_2O_3 and carbon powders was also used as the precursor material to fabricate Ga_2O_3 nanostructures [139–141]. The key growth parameters, including precursors, growth temperature, growth pressure, growth duration, and gas flow rate, as well as separation distance between the metal source and substrate, all play important roles in depositing Ga_2O_3. Mostly, β-Ga_2O_3 nanostructures in the forms of nanowires, nanobelts, and nanorods will be possibly obtained, determined by the vapor–liquid–solid (VLS) or vapor–solid (VS) growth mechanisms [11]. Figure 6b–e shows some newly CVD-deposited Ga_2O_3 nanostructures, such as nanowires, nanorods, nanobelts, nanoribbons, and core–shell nanowires in recent years. Although a large variety of Ga_2O_3 nanostructures can be grown epitaxially on substrates using CVD, its disadvantage is that a high operating temperature is required, and the by-product gas may be hazardous and harmful.

4.4. Sol–Gel Synthesis

Of all the solution synthesis approaches, the sol–gel method is the most extensively used method to synthesize metal oxide-sensing material, since it allows for exquisite control over the size, shape, and crystal phase of the resultant material. The sol–gel process usually involves several steps: (i) dispersion of colloidal particles in a liquid to form a sol, (ii) deposition of the sol solution on a substrate by spraying or dipping or spinning, (iii) polymerization of the particles in the sol to become a gel by stabilizing the removal of the component, and (iv) pyrolysis of the remaining organic or inorganic components, thus forming the final film. Inorganic metal salts or metal organic compounds, e.g., gallium

nitrate [142–145] and gallium isopropoxide [146–152], were commonly available precursor solutions used in the sol–gel process of Ga_2O_3-sensing material. The sol–gel synthesis of Ga_2O_3 films depends on the solvent, pH value, viscosity, temperature, and so on. The surface morphology and crystallinity can be modified by subsequent heat treatment. However, disadvantages such as weak adhesion and low wear resistance limit its application in sensor fabrication.

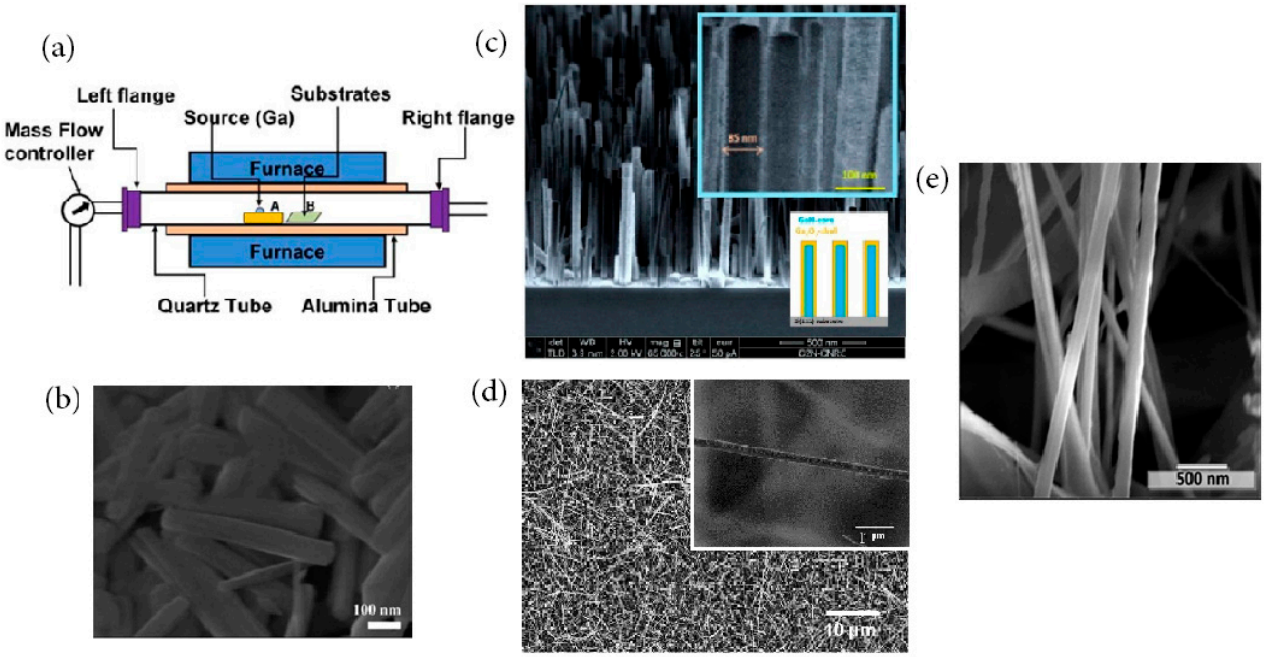

Figure 6. (**a**) Schematic experimental setup of the CVD furnace for the growth of Ga_2O_3 nanostructures [11]. Copyright 2013 Wiley. (**b**) SEM image of β-Ga_2O_3 nanorods [135]. Copyright 2016 The Royal Society of Chemistry. (**c**) SEM image of GaN/Ga_2O_3 core–shell nanowires [131]. Copyright 2019 MDPI. (**d**) SEM and HR-TEM images of β-Ga_2O_3 nanowires [140]. Copyright 2020 Elsevier. (**e**) SEM image of SnO_2-coated β-Ga_2O_3 nanobelts [132]. Copyright 2021 Elsevier.

4.5. Hydrothermal Synthesis

Due to easy operation and tunable growth parameters, hydrothermal synthesis is an important approach for the preparation of nanocomposites for gas sensor application. The hydrothermal process begins with an aqueous mixture of soluble metal salt precursors. Then, the solution is placed in an autoclave for reaction under relatively high pressure and moderate temperature conditions. In most cases, gallium nitrate hydrate $Ga(NO_3)_3 \bullet xH_2O$ [153–162] was used as the precursor for synthetizing Ga_2O_3 nanomaterials. The chosen solution has been always distilled water, while other organic solvent such as alcohol [156,157] was also used. After hydrothermal growth, the precipitates were calcinated for a couple of hours to improve the crystallinity. To obtain Ga_2O_3-sensing material with a certain size and morphology, it needs to precisely modulate the PH value and concentration of the solution, temperature, pressure, and reaction time. However, it is difficult to control the tailored phases and exact morphologies. Pilliadugula and Krishnan [159] studied the effect of PH on the surface morphology of hydrothermal synthesized β-Ga_2O_3 powders. Figure 7 shows the morphology evolutions of the as-prepared samples at different PH values. It was demonstrated that an extremely alkaline solution (PH = 14) caused higher-order hierarchical structures, whereas the acidic solution (PH = 5) facilitated nanorod structures. Cocoon-shaped morphology was formed as the PH value was increased from 7 to 11.

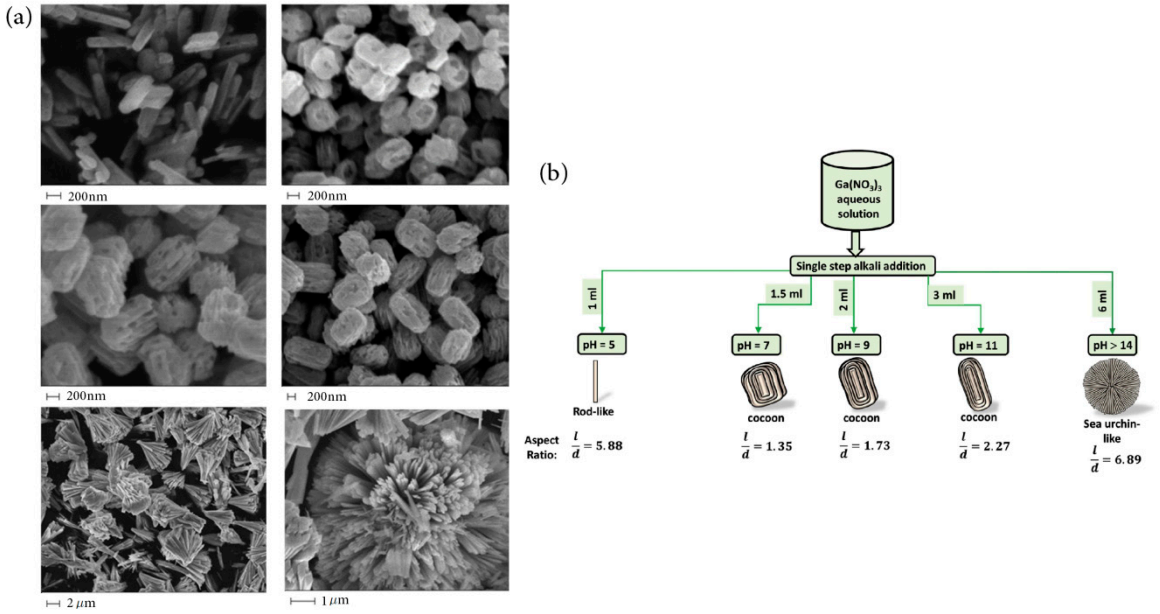

Figure 7. (**a**) SEM images of the morphological evolution of β-Ga_2O_3 nanostructures [159]. (**b**) Schematic representation of morphological evolutions at different pH values [159]. Copyright 2020 Elsevier.

4.6. Other Methods

Besides the above-discussed methods, there have been other vacuum and nonvacuum growth techniques, such as pulsed laser deposition (PLD) [163–167], atomic layer deposition (ALD) [168], coprecipitation [169,170], and spray pyrolysis [171], for the fabrication of Ga_2O_3-sensing material. Photoelectrochemical oxidation [172–174] was also used to grow Ga_2O_3 thin films on the GaN surface. In this process, the GaN epitaxial film was dipped into a phosphoric acid solution and then oxidized under the illumination of a He-Cd laser source with wavelength of 325 nm. An amorphous Ga_2O_3 film was directly grown and could be converted to the β-Ga_2O_3 phase by annealing in O_2 or N_2 ambiance. Recently, a novel liquid gallium-based sonication approach [175–177] was developed to prepare Ga_2O_3 thin films with lots of microparticles. Using this approach, ternary alloy oxides with tuning compositions were achieved by the probe sonication of liquid gallium with traces of In, Sn, and Zn in the water medium or other solvents. After annealing, the as-prepared samples can be applied for sensing NO_2 at a low temperature.

5. Ga_2O_3-Based Gas Sensors

Over the past three decades, several types of gas sensors using Ga_2O_3 bulk crystals, thin films, and nanomaterials have been developed to detect diverse oxidizing and reducing gases during a wide operational temperature range from room temperature to more than 1000 °C. In this section, we will focus on the advances in Ga_2O_3-based gas sensors, which cover the fundamentals of semiconductor metal oxide gas sensors and the prevailing strategies for how to improve the performance of Ga_2O_3 gas sensors.

5.1. Sensing Mechanisms

Gas-sensing mechanisms explain why the gas can cause changes in the electrical properties of a sensor. Several common gas-sensing mechanisms of metal oxide semiconductor gas sensors were reviewed by Ji et al. [178] in detail. However, the mechanisms governing Ga_2O_3-based gas sensors seem quite different. Most gas sensors using Ga_2O_3 are based on the resistive or conductive change upon target gas exposure. The sensing mechanisms of conductivity for Ga_2O_3-based gas sensors can be found in Refs. [3,26,179–181]. As mentioned above, the conductance of n-type Ga_2O_3 is determined by the carrier concentration

and electron mobility. Both of them are temperature-dependent. When detecting gas, the change in conductance of Ga_2O_3 is dominated by the variation of electron density at a high temperature, while the influence of the conductance of Ga_2O_3 from electron mobility at a low temperature is more distinctive. As far as the mechanism that describes the interaction between the target gas and the sensitive metal oxide is concerned, three temperature-dependent regimes can be distinguished for Ga_2O_3-based resistive gas sensors [4,26,179–182] from Figure 8a.

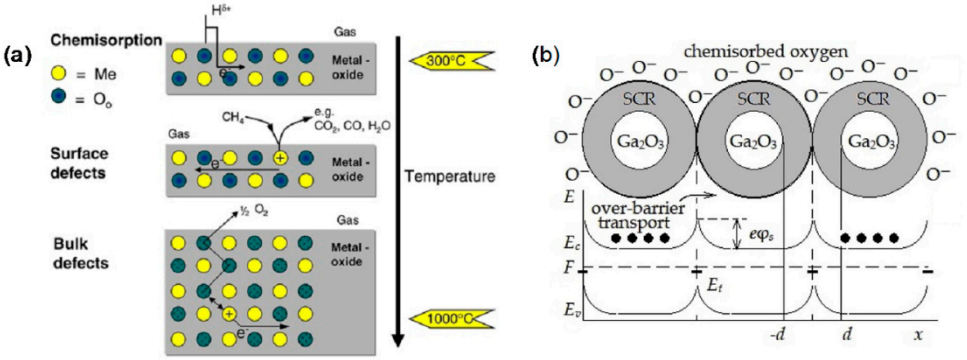

Figure 8. (**a**) The model of the three temperature-dependent regimes of the gas reaction of Ga_2O_3 [182]. Copyright 2008 IOP. (**b**) The model and corresponding energy diagram of Ga_2O_3 grain contact [87]. Copyright 2020 Elsevier.

In a high operating temperature range above 800 °C, the oxygen in the surrounding atmosphere and in the crystal lattice is in dynamic equilibrium, which means the oxygen exchange undergoes constantly between the bulk lattice of Ga_2O_3 and the ambient. If there is a reduction in the proportion of oxygen in the surrounding atmosphere, Ga_2O_3 crystal will experience an increase in the concentration of positively ionized oxygen defects in the lattice. Using the Kröger–Vink notation, the sum of the processes can be described as [180]

$$Ga_2O_3 \leftrightarrow 2Ga_{Ga}^{x} + 2O_O^{x} + V_O^{*} + e^{-} + 1/2O_2^{(g)}. \quad (2)$$

As a consequence, the conductivity of Ga_2O_3 increases because of the delocalized electrons in crystal lattice. It can be said that this sensing regime is dominated by bulk oxygen defects. One can use it to implement high temperature oxygen sensors, which obey a typical power law [26,99,183]

$$\sigma \propto p_{O_2}^{m} e^{-E_A/kT}, \quad (3)$$

where p_{O2} is the oxygen partial pressure and E_A is thermal activation energy of a dopant, k is the Boltzmann constant, and T is the temperature. The first part in above equation represents the contribution from the oxygen partial pressure, and the last part reveals the temperature dependence of the conductivity on the doped specimens.

In the intermediate operation temperature range below 800 °C, only an exchange of oxygen near the surface of Ga_2O_3 with the surrounding gas takes place. If a certain reducing gas such as CH_4 approaches the surface, it will be oxidized by oxygen from the near-surface region, leading to the formation of oxygen vacancy donors at surface and a greater conductivity due to the release of conduction electrons. The process then will be recovered in the absence of reducing gas, since the loss of oxygen of the Ga_2O_3 surface is compensated by the oxygen from the ambient atmosphere. In this case, the sensing regime is mainly caused by surface oxygen defects.

At even lower temperatures, the oxygen defect equilibrium disappears. The gas-sensing behavior is dominated by the change in electron mobility controlled by grain boundaries, rather than the change in oxygen defect-affected charged carrier density. As shown in Figure 8b, on the one hand, similar to other metal oxides, a potential barrier is formed at the grain boundary of Ga_2O_3 by pre-adsorbed oxygen ions with negative charge in the air, leading to a charge depletion region between grains. The adsorbed oxygen ions

are O_2^- below 200 °C, O^- in the range of 200–550 °C, and O^{2-} above 550 °C. The width of charge depletion region is determined by the Debye length [26]:

$$L_D = \sqrt{\varepsilon kT/ne^2}, \quad (4)$$

where ε is the permittivity, n is the electron density, and e is the electronic charge.

When exposed to a reducing gas such as CO, the gas molecules react with chemisorbed oxygen ions at the Ga_2O_3 surface and return the captured electrons to the conduction band, resulting in the decrease of the depletion width. Hence, the conductance is increased due to the easier electronic transport across the grain boundary. In the case of the presence of an oxidizing gas such as NO_2, a competitive adsorption process may take place, and the overall results are a wider depletion region, smaller electron mobility, and a decrease of conductivity. However, the sensitivity toward NO_2 could be very low, since the Debye length of Ga_2O_3 is as large as several μm [181].

On the other hand, reducing a gas such as H_2 will be chemisorbed at the surface via covalent bonds to form adsorbed molecules with positive charges. To satisfy the electric neutrality, more conduction electrons are released, yielding a conductive increase in n-type Ga_2O_3. The chemisorption process happens even with no oxygen in the ambient. However, the overall concentration of the surface adsorbed species is subject to the Weisz limit [184]. Clearly, gas chemisorption and reaction at the surface play an important role in this low-temperature-sensing regime.

It should be noted that there are no upper and lower temperature limits for the three gas-sensing regimes. The modulation of the conductance of Ga_2O_3 by the target gas can be a consequence of one or a combination of grain boundaries, gas absorption and reaction, and oxygen vacancies. There have also been various Ga_2O_3-based nonresistive gas sensors using different operating principles. For example, the gas-induced changes in work function, in capacitance, in the Schottky potential barrier, and in the ionic conductivity can be used for sensing a wide range of target gases. These gas-sensing mechanisms are similar to those of other semiconductor metal oxide sensors, which can be easily found in a lot of the literatures such as [185].

5.2. Evaluation Criteria

Usually, the performance of Ga_2O_3-based gas sensors can be evaluated with respect to the '4s'-criteria: sensitivity, speed, selectivity, and stability [43].

The sensitivity S, also named as response, in the presence of gases is usually defined in several different forms. It is generally calculated from the ratio of the electrical readout (resistance R or conductance G and current I or volt V) of the sensor in background gas (usually air) Y_a to that upon exposure to certain concentrations of the target analyte Y_g:

$$S = Y_a/Y_g, \quad (5)$$

for oxidizing the target gas and

$$S = Y_g/Y_a, \quad (6)$$

for reducing the target gas.

Other expression forms of sensitivity that describes the variation degree of the output signal are also in use:

$$S = \Delta Y_a/Y_g. \quad (7)$$

The detection speed is evaluated by the response and recovery time. The response time is defined as the time required for a sensor to reach 90% of the total response upon exposure to the target gas. Recovery time is defined as the time required for a sensor to return to 90% of the original baseline signal upon removal of the target gas.

The selectivity of a sensor describes how much the sensor is disturbed by interfering gases from the target gas. The selectivity Q, which reflects the ability of a sensor to

differentiate between the target gas x and the other components in the gaseous environment x′, can be expresses as:

$$Q = S_x / S_{x'}. \quad (8)$$

Obviously, larger Q means better selection of target gas and stronger resistive to interfering gas.

The stability (reproducibility) describes the endurance of a gas sensor to maintain its output signal over a long period of time and/or to the analyte gas of varying concentrations. The stability is greatly affected by thermal aging and gaseous poisoning of the sensor layer, especially when operating in a harsh environment.

Additionally, the operating temperature, power consumption, size, and cost are the other concerns that should be considered, depending on particular applications of gas sensors. It is difficult to achieve all the optimal results of the above performance parameters at the same time. Therefore, to keep the balance according to the specific situation and requirements has become a major aim for the development of Ga_2O_3 gas sensors.

5.3. Classification of Ga_2O_3-Based Gas Sensors

According to the famous Yamazoe model [186], a gas sensor can be considered as an integration of a receptor and a transducer. The former is provided with a material or a material system that interacts with a target gas and thus induces a change in its own properties or emits heat or light. The latter is a device to transform such an effect into an electrical signal. There are various approaches used for gas sensor classification. In terms of transduction principles, the gas sensors that many groups have always developed using Ga_2O_3 as sensing materials can be classified into three categories: electrical gas sensors, electrochemical gas sensors or solid electrolyte-based gas sensors, and optical gas sensors [187].

5.3.1. Electrical Gas Sensors

Electrical gas sensors, operating due to electronic conduction induced by a surface interaction with target gas, contain resistor-type gas sensors and nonresistive sensors such as SBD-, FET-, and capacitor-type gas sensors.

(1) Resistor-type gas sensors are the conductometric sensors that measure the change in resistance caused by the interaction between the sensing element and analyte gas. They possess advantages such as simple configuration, easy fabrication, and cost effectiveness and can be easily miniaturized and integrated on a microelectronic mechanical system platform. A typical resistor-type gas sensor based on Ga_2O_3 is depicted in Figure 9a. Pt and Au are commonly used as measuring electrodes, since the electron affinity of Ga_2O_3 is as large as about 4 eV [40]. Similar to solar-blind ultraviolet photodetectors, the interdigitated electrode geometry, which enables a wide contact area, is the most widely accepted geometry for a resistor sensor. In most cases, it forms the electrodes first and then deposits the Ga_2O_3-sensing layer on them, thereby causing no damage to the sensing material. Additionally, a Pt heater is placed on the back side of the substrate to heat the sensor.

In early years, Fleischer and Meixner in Siemens AG and their cooperators adopted the RF magnetron sputtering technique to fabricate β-Ga_2O_3 polycrystalline thin films and constructed resistor sensors to detect a variety of gases, such as O_2 [41,42,74,79,96,102,188–190]; O_3 [81]; H_2 [74,78,79,82,89,90,95,191–194]; CO [75,79,82,89,91,97,188,189,191,192]; NO [78,79,96]; NH_3 [79,96]; and hydrocarbons (HCs) such as CH_4 [73,77–79,82,94,97,102,188,189,195], C_3H_8 [79,82,196], and C_4H_8 [79,188], as well as volatile organic compounds (VOCs) such as C_2H_6O [78,79,97,195] and C_3H_6O [78,80,82]. The operating temperature ranges from 1100 °C to 400 °C. Typically, polycrystalline Ga_2O_3 thin films can be used either for sensing oxygen (>900 °C) or reducing gases (<900 °C) [14,91]. The co-adsorption of H_2O and other coexisting gases of the sputtered films were considered by Giber et al. [197], Reti et al. [198–200], and Pohle et al. [201]. Due to a high operating temperature, a self-cleaning effect was observed on the sensor surface, and the unwanted species could

be eliminated to a large extent. Varhegyi et al. [202] investigated the influence from corrosive gases such as Cl_2 and SO_2 on the Ga_2O_3-sputtered layer and found that Ga_2O_3 was more resistant against SO_2 but had a very fast reaction with Cl_2 at 800 °C. A screen-printing technique was developed by Frank et al. [188], Pole et al. [201], Wiesner et al. [195], and Biskupski et al. [196] to prepare porous Ga_2O_3 thick films for detecting oxidizing gases such as CO_2 and O_3 and inflammable gases such as C_4H_{10} and C_3H_8, as well as VOCs. Additionally, many other groups such as Macri et al. [72], Ogita et al. [62,63,97,103], Hovhannisyan et al. [203], Dyndal et al. [204], Almaev et al. [86,87], Manandhar et al. [101], and Sui et al. [64] studied the gas sensitivities of resistor sensors with sputtering films for O_2, H_2, CO, C_7H_8, C_2H_6O, and C_3H_6O. However, it is very hard to reduce the operating temperature of these resistor sensors using the Ga_2O_3 compact films to a lower value.

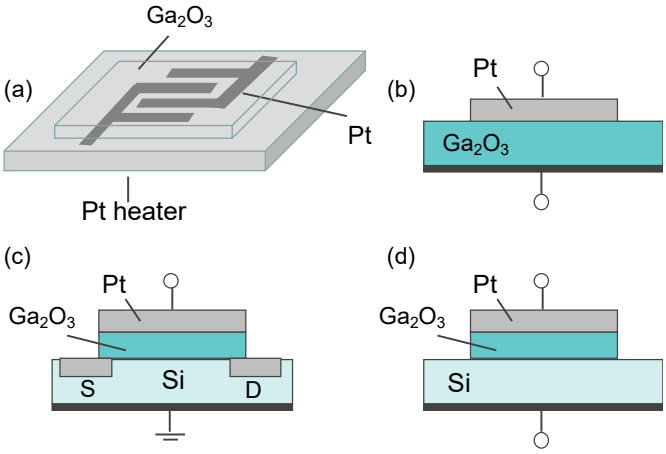

Figure 9. Schematic device structures for (**a**) resistor-type (**b**) SBD-type, (**c**) FET-type, and (**d**) capacitor-type Ga_2O_3-based gas sensors. Redrawn with permission from G. Korotcenkov [187]. Copyright 2014 Springer.

With the progress of advanced synthesis technologies, many novel Ga_2O_3 nanomaterials with different compositions and microstructures have been prepared for resistor sensors. The morphology of these Ga_2O_3 functional nanomaterials varies from one dimensional to three-dimensional nanostructures such as nanospheres, nanoflowers, nanowires, nanorods, nanobelts, and so on. These sensing materials showed high resistive response towards O_2 [109], CO [109,124,129,135,140,154,155], CO_2 [158], H_2 [113,132,176], NH_3 [159,162,177], NO_2 [125, 126,128,141,160,161,176], VOCs such as C_2H_6O [117,123,141,168], C_3H_6O [123,133,157], C_3H_8O [120], and water vapor [127,130,134], as reported by many authors. The operating temperature can be low to room temperature due to the large specific surface area and robust properties of nanostructures.

(2) Since Lundstrom et al. [205] first achieved a H_2-sensitive Pd-gate gasFET device, there has been of great interest in semiconductor metal oxide nonresistive-type gas sensors due to the simple electrical circuit required to operate them. In contrast to the above-discussed resistor-type gas sensors, the gas-sensing properties of nonresistive ones will be less affected by the morphology of Ga_2O_3-sensing material. In generally, nonresistive type gas sensors consist of two types of structures, i.e., metal/semiconductor (MS) is metal/insulator/semiconductor (MIS) structures. Comparatively, the MIS structure is always adopted in designing Ga_2O_3 sensors with Pd or Pt as catalytic metals and Ga_2O_3 as reactive insulator material. There are usually three types of nonresistive-type gas sensors based on various operating principles, namely, SBD-type, FET-type, and capacitor-type gas sensors. Figure 9b–d depict the schematic device structures of these three typical Ga_2O_3-based nonresistive-type gas sensors. The basis with respect to SBD- or FET-type (including MIS capacitor) gas sensors with a catalytic metal is modulation in the Schottky barrier height or the flat band potential by target gas [187]. Catalytic decomposition of hydrogen on the surface of noble metal and subsequent diffusion of hydrogen atoms to

the interface between metal and insulator make these devices respond to H_2 and many hydrogen containing gases.

SBD-type sensors operate on the change in Schottky barrier height affected either by formation of a dipole layer or by modification of work function once gaseous species interact with the metal surface. Then, the gas-induced rectifying property can be recognized by I–V characteristics under a forward, as well as reverse, bias voltage. Pt/Ga_2O_3/SiC [146,149–152] and Pt/Ga_2O_3/GaN [172–174] Schottky diode gas sensors were built to detect H_2 and C_3H_6 at different operating temperatures. Notably, Jang et al. [52] and Nakagomi et al. [68,69] reported Schottky diode gas sensors based on β-Ga_2O_3 single crystals, which showed an enhanced response to H_2 and stable operation at elevated temperatures. Almaev et al. [136] studied the gas-sensing properties of Pt/α-Ga_2O_3: Sn/Pt Schottky metal–semiconductor–metal structures when exposed to H_2, O_2, CO, NO, CH_4, and NH_3 in the temperature range of 25–500 °C.

FET-type sensors are based on the readout of work function change of the sensing material. The gas response of FET-type sensors is measured as a shift in either gate-source voltage or drain-source current, and it has been shown that this response is related to a shift in the threshold voltage. This kind of gas sensors can detect many reducing gases, such as H_2 and VOCs. A hybrid FET-type sensor was designed using Ga_2O_3 as the sensitive layer and the measured variation of the work function indicated a multiple response to H_2, NH_3, and NO_2 [206–208]. In their work, an analytic theoretical model was proposed to explain the inner sensing mechanism. Lampe et al. [84] made a gas FET sensor in which a sputtered Ga_2O_3 thin film activated with Pd was used to detect CO. Stegmeier et al. [85,86] used sputtered Ga_2O_3 film to construct a FET-type sensor for detecting VOCs. Nakagomi et al. [118,119] reported a field–effect hydrogen sensor using Ga_2O_3 thin film prepared by CVD. Shin et al. [209] investigated the channel length scaling effects on the signal-to-noise the ratio of a FET-type NO_2 sensor. It was demonstrated that the FET gas sensors had an advantage of working at room temperature.

MIS capacitor-type sensors are changes that can be made to the relative permittivity of the dielectric, the area of the electrode, or the distance between the two electrodes and, therefore, by measuring the change in the capacitance. Arnold et al. [110] reported an interdigital comb-finger structural capacitor gas sensor with β-Ga_2O_3 nanowires as dielectric. By capacitance measurement using a balanced AC bridge circuit, the sensor showed a rapid and reversible response to VOCs such as C_2H_6O and C_3H_6O and a more limited response to some HC_s, including C_7H_8 at room temperature. Mazeina et al. [114,115] compared pure and functionalized Ga_2O_3 nanowires as active material in room temperature capacitance-based gas sensors. It was found that the functionalization of Ga_2O_3 nanowires with acetic acids showed a significant decrease in response to C_3H_8O and CH_3NO_2 as well as $C_6H_{15}N$. In the case of pyruvic acid-functionalized nanowires, no response was observed to CH_3NO_2, but one order of magnitude increased response to $C_6H_{15}N$ was obtained compared to the pure nanowires.

5.3.2. Electrochemical Gas Sensors

An electrochemical gas sensor is a device that yields an output as a result of an electrical charge exchange process at the interface between ionic or electronic conductors. Solid electrolytes exhibit high ionic conductivity resulting from the migration of ions through the point defect sites in their lattices. In solid electrolyte-based sensors, electronic conduction only makes typically less than 1% contribution to the total conductivity, while the ionic conductivity contributes to 99% of the rest. Schematic device structures for two kinds of electrochemical gas sensors containing Ga_2O_3 are shown in Figure 10. In an early study, NH_4^+ ion conducting gallate solid electrolyte was prepared by mixing K_2CO_3, $RbCO_3$, and Ga_2O_3 [210]. Fabricated by the combination of NH_4^+-Ga_2O_3 and rare earth ammonium sulfate as a solid electrolyte and a solid reference electrode, the gas sensor showed outstanding NH_3 detection in good accordance with the Nernst relation. In a mixed potential gas sensor based on O^{2-} ion conducting yttria-stabilized zirconia (YSZ)

solid electrolyte, Ga_2O_3 was used to stabilize the metal (Au, Pt) electrode in its morphology and to inhibit its catalytic activity [211–215]. The results indicated that these gas sensors had a high sensitivity and good selectivity of HCs, such as C_3H_6. An electrochemical Pt/YSZ/Au-doped Ga_2O_3 impedance metric sensor was fabricated by Wu et al. [216]. The impedance of the sensor originated from the Ohmic contact resistance, the electrolyte impedance, and the interfacial impedance between the electrolyte and the sensing electrode. Strong dependence of the interfacial impedance upon the CO concentration at 550 °C was found due to an electrochemical oxidation of CO. Yan et al. [217] synthesized a mesoporous β-Ga_2O_3 nanoplate to make an amperometric electrochemical sensors. It was summarized that more oxygen defects and action sites in β-Ga_2O_3 nanoplate account for enhanced gas sensitivity in detecting CO.

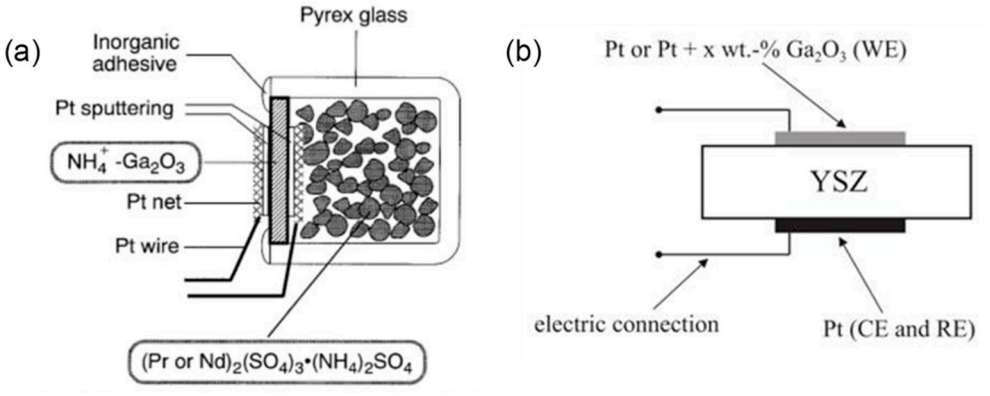

Figure 10. Schematic device structures for electrochemical gas sensors: (**a**) NH^{4+}-Ga_2O_3 solid electrolyte [210] Copyright 1998 The Electrochemical Society. (**b**) YSZ solid electrolyte [214]. Copyright 2004 Elsevier.

5.3.3. Optical Gas Sensors

Optical gas sensors detect changes in visible light or other electromagnetic waves during interactions with gaseous molecules. Reiprich et al. [122] used a corona discharge assisted growth morphology to prepare Sn-doped Ga_2O_3 for optical gas-sensing application. The Sn-doped Ga_2O_3 layer was shown to be capable of detecting small amounts of C_2H_6O, C_3H_6O, and C_3H_8O at room temperature. The reason was that the generation and quantity variance of negatively charged oxygen ions indirectly produced a change in the photoluminescence spectrum. It was also observed that the response toward C_3H_6O of a Ga_2O_3 layer-like structure would be increased by 30% relative to the nanowires. However, the study of Ga_2O_3-based optical gas sensors is in its infancy, further careful investigations are needed into this type of gas sensor.

To sum up, Ga_2O_3-based gas sensors exhibit broad-range sensitivity to a wide variety of analyte gases. Table 3 lists the available target gases of different types of Ga_2O_3-based gas sensors. The most preferable target gases are O_2, CO, H_2, and CH_4 [218].

Table 3. Target gases of Ga_2O_3-based gas sensors.

	Electrical Gas Sensors				Electrochemical Gas Sensor	Optical Gas Sensor
	Resistor	**SBD**	**FET**	**Capacitor**		
Environmental gases	O_2, CO_2, O_3, NH_3, SO_2	O_2, NH_3	NH_3		NH_3	
Highly toxic gases	CO, H_2S, NO, NO_2	CO, NO	CO, NO_2		CO	
Combustible gases	H_2, CH_4, C_4H_{10}, C_3H_8, C_4H_8, C_7H_8	H_2, CH_4, C_3H_6	H_2	C_7H_8	C_3H_6	
VOCs	C_2H_6O, C_3H_6O, C_3H_8O			C_2H_6O, C_3H_6O, C_3H_8O		C_2H_6O, C_3H_6O, C_3H_8O
Humidity	H_2O					
Other gases	C_2H_6S			CH_3NO_2, $C_6H_{15}N$		

5.4. Performance Enhancement Strategies

As is discussed in the former section, Ga_2O_3 can be used to make several types of gas sensors that respond to lots of gases, ensuring a wide application range. However, Ga_2O_3-based gas sensors still encounter some issues such as low selectivity, average sensitivity, and high operation temperature [26,182,187,218]. Multiple ways have been developed till now by many researchers to improve the gas-sensing performance of Ga_2O_3-based gas sensors through material engineering and device optimization.

5.4.1. Surface Modulation of Pure Ga_2O_3

It is well-known that the performance of Ga_2O_3 gas sensors greatly depends on the interaction between target gas and the Ga_2O_3 surface. Therefore, surface modulation, such as crystallinity, porosity, and oxygen vacancies, in the process of fabricating Ga_2O_3-sensing material plays an important role in determining the gas-sensing behavior. Ogita et al. [63,67,99,100,219] presented a series of studies on the influence of the annealing conditions on the high-temperature oxygen-sensing properties of the Ga_2O_3 thin film sensor. The results indicated that the annealing conditions affect not only the grain size, number of oxygen vacancies and surface roughness but also the oxygen-sensing properties of Ga_2O_3 thin films. The oxygen sensitivity of the sensors increases when the oxygen flow rate was increasing from 0 to 100% at 1000 °C. The response time of the Ga_2O_3 sensors decreased as the grain size increases with increasing the annealing temperature and annealing time. The authors also measured the oxygen-sensing characteristics at 1000 °C for β-Ga_2O_3 sputtered thin films and β-Ga_2O_3 single crystals and found that both sensors had response times in the same range. Grain boundaries played an important role in determining the value of the response time in sputtered films, while the surface processes primarily influenced the modifications of the resistance for single crystals. The influence of film thickness on sensing response at room temperature was investigated by Pandeeswari and Jeyaprakash [171]. The sensitivities towards 0.5 ppm and 50 ppm of NH_3 increased as the film thickness became larger.

Due to large surface to volume ratio and abundant surface active sites to the target gas, porous and nanostructured Ga_2O_3 was always used as the sensing layer. Cuong et al. [113] addressed the effect of growth temperature on the microstructural properties and H_2 sensing ability of Ga_2O_3 nanowires. Girija et al. [135] performed the gas-sensing analysis of morphology-dependent β-Ga_2O_3 nanostructure thin films. It can be seen from Figure 11 that nanorods of β-Ga_2O_3 had a higher surface area with a larger pore volume distribution than rectangular β-Ga_2O_3 structures. As a result, rod shaped β-Ga_2O_3 nanostructures showed better sensitivity, shorter response, and recovery time upon exposure to CO gas at 100 °C in comparison with rectangular shape β-Ga_2O_3 nanostructures. The improvement on sensor performance could be contributed from the high surface area, particle size, shape, numerous surface active sites and the oxygen vacancies. The effect of pH-dependent morphology evolutions on room temperature NH_3-sensing performances of β-Ga_2O_3 nanostructured films was investigated by Pilliadugula and Krishnan [159]. It could be seen that the sample with hierarchical morphology and relatively low crystallite size showed utmost sensing responses at all concentrations of NH_3 relative to the remaining samples.

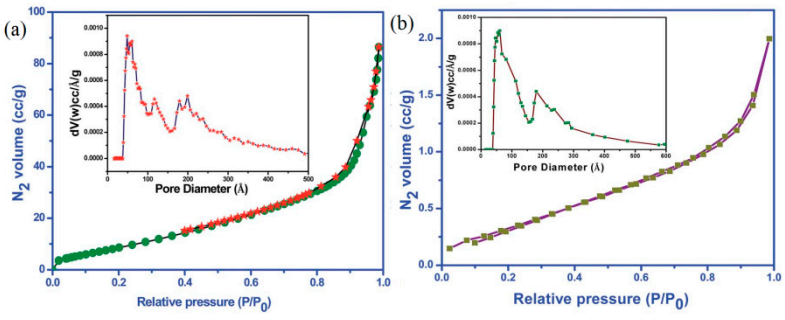

Figure 11. *Cont.*

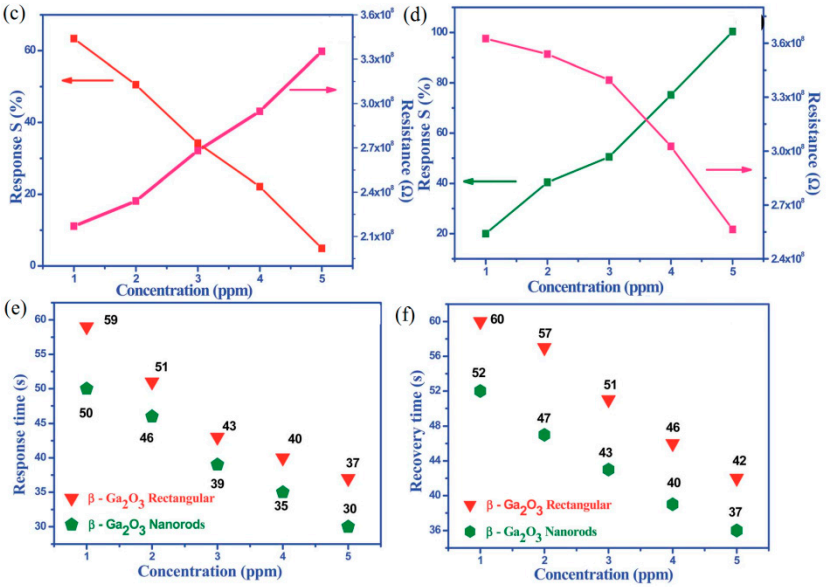

Figure 11. Nitrogen adsorption-desorption isotherm of the Ga_2O_3 (**a**) rectangular and (**b**) rod-shaped nanostructures (inset: the corresponding pore size distribution). Sensing response and electrical resistance as a function of CO concentration at 100 °C (**c**) β-Ga_2O_3 rectangular nanorods, (**d**) β-Ga_2O_3 nanorods, (**e**) response time, and (**f**) recovery time of different β-Ga_2O_3 nanostructure thin films [135]. Copyright 2016 The Royal Society of Chemistry.

High-energy crystal facet has a higher surface energy and more defect sites, thus exhibiting more active physicochemical properties and better gas-sensing performance. Jang et al. [52] demonstrated that the H_2 responses of the (010) facet were slightly higher than that of the ($\bar{2}$01) facet when studying the sensing characteristics of Schottky diode-type gas sensors using Ga_2O_3 single crystal. However, it is not clear which facet is the most active one for gas sensors so far.

5.4.2. Sensitizing by Noble Metal

In most of gas-sensing process, small noble metal nanoparticles or clusters distributed on the surface of Ga_2O_3 can improve the efficiency of catalytic reactions between target gases and the surface of sensing layers, thus remarkably enhancing the gas-sensing characteristics. At an early stage, Fleischer et al. [91], Bausewein et al. [74], and Schwebel et al. [75] studied the effects of Pt, Pd, and Au catalyst dispersions on the sensitivity to reducing gases of high temperature Ga_2O_3 thin film sensors. They found that Pt dispersion accelerated the response of CO, whereas significantly increased the sensitivity to H_2. Au clusters on the Ga_2O_3 surface could yield a high sensitivity to CO and a distinct reduction of the cross-sensitivity towards VOCs. However, although Pt accelerated the desorption of H_2 on Ga_2O_3, it had no impact on the sensitivity to H_2. Recently, Krawczyk et al. [138] reported the impregnation of Au nanoparticles of the HVPE-prepared n-type β-Ga_2O_3 layer would cause an inversion to p-type conductivity at the surface. The conductive sensitivity of the Au-modified β-Ga_2O_3 layer toward 16 ppm of dimethyl sulfide obviously was enhanced if compared to that of the unmodified β-Ga_2O_3 layer. Pt and Au-decorated Ga_2O_3 nanowires were synthesized by Kim et al. [124] and Weng et al. [140]. Figure 12 shows the SEM and TEM images and electrical response of the gas sensors fabricated by Pt- and Au-decorated Ga_2O_3 nanowires. As measuring at 100 °C, the responses of the Pt-functionalized nanowire were reported to improve 27.8-, 26.1-, 22.0-, and 16.9-fold at CO concentrations of 10, 25, 50, and 100 ppm, respectively, relative to the bare Ga_2O_3 nanowires. However, both the response and recovery times of this Pt-functionalized CO sensor were increased significantly. Through CO gas sensor measurements at room temperature, Au-decorated single β-Ga_2O_3 nanowire showed better results than single pure β-Ga_2O_3 nanowire and multiple networked Au-decorated β-Ga_2O_3 nanowires. The enhancement of the CO-sensing proper-

ties was resulted from a combination of the spillover effect and the enhanced chemisorption and dissociation of the target gas.

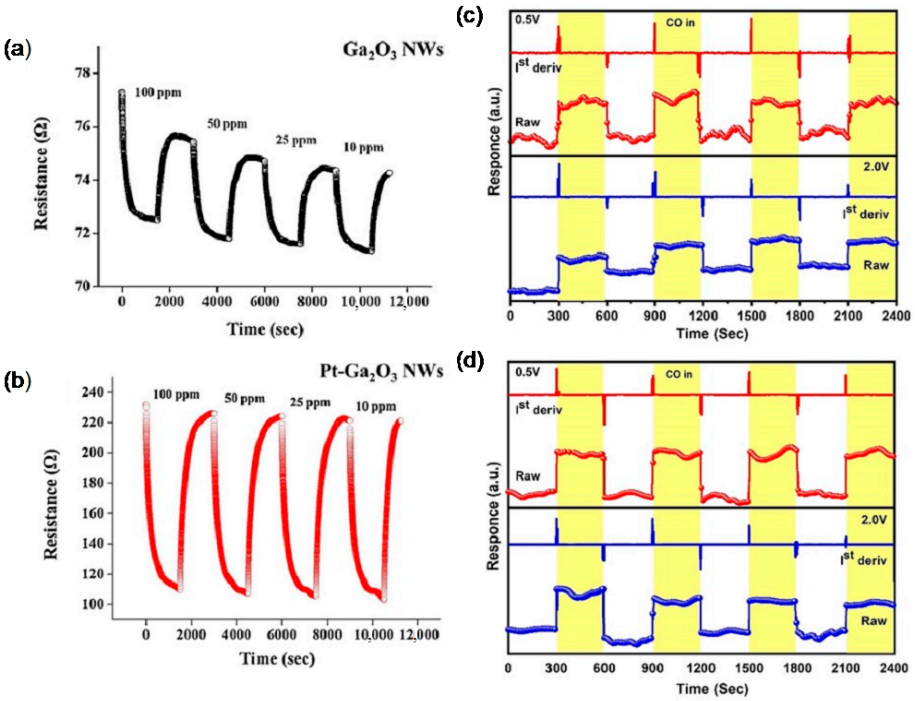

Figure 12. Gas responses of (**a**) bare Ga_2O_3 nanowires and (**b**) Pt-coated Ga_2O_3 nanowires to 10, 25, 50, and 100 ppm CO gas at 100 °C [124]. Copyright 2012 Elsevier. Room temperature CO gas sensor measurement results with different bias voltages for (**c**) pure β-Ga_2O_3 nanowires and (**d**) Au-decorated β-Ga_2O_3 nanowire with 2158 ppm CO concentration [140]. Copyright 2020 Elsevier.

So far, noble metals had also been used in FET-type and solid electrolyte type gas sensors to catalytically activate the sensing layer. Zosel et al. [212,213] achieved a high sensitivity for hydrocarbons in potentiometric zirconia-based gas sensors, attributed to the catalytic activity of the Au composites. Shuk et al. [215] reported that the mixed potential solid electrolyte sensor based on Au/Ga_2O_3 composite electrodes had a sensitivity limit of 5 ppm CO and showed good selectivity, reproducibility, and stability in the presence of other combustion gas species. The FET-type sensors thermally activated by Pd and Pt for the detection of reducing gases were studied by Lampe et al. [84] and Stegmeier et al. [85,86]. The results indicated that catalytic Pt dispersions on the micro- and nanoscale caused a remarkable gas response at room temperature to a large variety of hydrocarbons and VOCs with small concentrations (ppb-ppm). Overall, noble metals such as Pt, Pd, and Au play the roles of chemical sensitizers and electronic sensitizers in Ga_2O_3 sensors.

5.4.3. Doping Specific Element

Doping is an effective way to influence not only the electronic properties but also the structural properties of grains, such as size and shape, leading to the enhancement of sensing behavior. Frank et al. [102,188,189] found that the doping of sputter-deposited polycrystalline Ga_2O_3 thin films using donor type ions such as Zr^{4+}, Ti^{4+}, and especially Sn^{4+} caused a modulation of the base conductivity by two orders of magnitude and strong impact on the sensitivity to reducing gases. However, there was no influence on the sensitivity to reducing gases such as CH_4 and CO after doping Mg^{2+} in the Ga_2O_3 and no influence of whether donor-type or acceptor-type doping concentration on O_2 sensitivity at high temperature. However, in the work of Almaev et al. [87,88], the authors stated that addition of Cr stimulated dissociative adsorption of O_2 due to its high catalytic activity via a spillover mechanism, leading to a significant increase in the response of to O_2 over the temperature range 250–400 °C. The O_2 gas-sensing performance of Ga_2O_3

semiconducting thin films prepared by the sol–gel process and doped with Ce, Sb, W, and Zn was investigated by Li et al. [148]. The authors observed that the operating temperature of sensors doped with Zn reduced below 450 °C and Sensors doped with Ce had a very fast response time of typically 40 s. W-doped sensors showed the highest response to O_2 while Sb-doped films possessed the highest base resistance. Sn was proven to be the most effective dopant in Ga_2O_3 for gas detection at different operating temperatures [121,122,162,170,189]. As examples, Figure 13 exhibits the enhancement of the sensor sensitivity of Sn-doped Ga_2O_3 gas sensors when detecting different gases. An increase in conductivity of up to two orders of magnitude, as well as an enhancement of the gas sensitivity toward CO and CH_4, was found by employing SnO_2 as a doping material into sputtered polycrystalline Ga_2O_3 thin films [189]. Doping Sn could enhance the adsorption of NH_3 due to the higher Lewis acidity of Sn^{4+} cations than Ga^{3+} ones [170]. Moreover, the introduction of Sn causes a decrease in the average crystallite size and an increase in the specific surface area [162]. Therefore, Sn-doped Ga_2O_3 NH_3 sensor showed better performance than the pure Ga_2O_3 one regardless of the operating temperature. Manandhar et al. [101] demonstrated that the Ti-doped nanocrystalline β-Ga_2O_3 films significantly accelerated the oxygen response about 20 times while retaining the stability and repeatability.

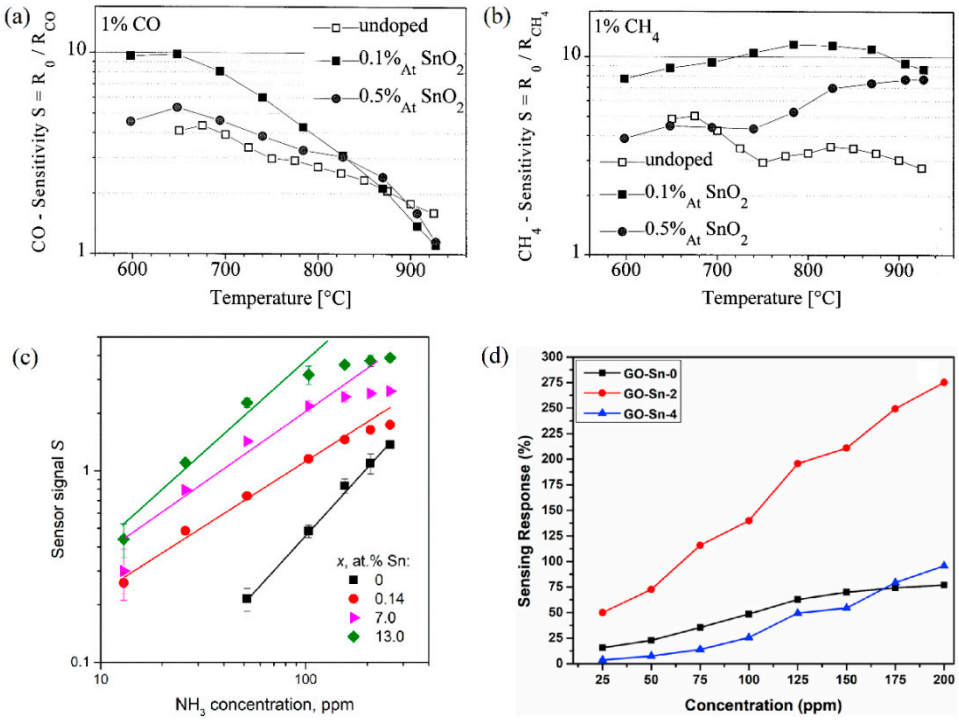

Figure 13. Enhancement of the sensitivity to (**a**) 1% CO and (**b**) 1% CH_4 of Sn-doped Ga_2O_3 thin films compared to undoped films [189]. Copyright 1998 Elsevier. (**c**) Sensor signal as a function of NH_3 concentration for Sn-doped Ga_2O_3 samples measured at 500 °C [170]. Copyright 2021 MDPI. (**d**) Room temperature-sensing response as a function of NH_3 concentration [162]. Copyright 2021 Elsevier.

It is noted that doping can not only enhance the sensing properties of resistor-type Ga_2O_3 sensors but also have a great impact on design of novel sensors. Reiprich et al. [122] used Sn-doped Ga_2O_3 nanostructure for optical gas-sensing at room temperature. The change in the photoluminescence spectra indicated that Sn-doped Ga_2O_3 was capable of detecting trace amounts of VOCs such as C_2H_6O, C_3H_6O, and C_3H_8O. Saidi et al. [176] developed a novel liquid metal-based ultrasonication process within which additional metallic elements (In, Sn, and Zn) were incorporated into liquid Ga and then sonicated in dimethyl sulfoxide (DMSO) and water. These new types of doped Ga_2O_3 sensors showed very tuning sensitivities to NO_2 and H_2. Impedance measurements were performed on the

Pt/YSZ/Au-doped Ga_2O_3 CO electrochemical sensor [216] and on the humidity sensor-based on Ga_2O_3 nanorods doped with Na^+ and K^+ [220]. Both types of Ga_2O_3 gas sensors showed fast response of target gases. Due to the synergistic effect of Ga_2O_3 nanorods and the doping of alkali metal ions, Ga_2O_3 nanorod gas sensor exhibited good linearity response and high stability over 25 days. So far, the dopants added in Ga_2O_3 were Zr, Ti, Mg, Sn, Ni, N, Na, K, Cr, In, Zn, Pt, and Au for the purpose of enhancing the sensing properties.

5.4.4. Constructing Ga_2O_3 Heterostructure

Semiconducting heterostructures show great potential in gas sensors because of a high surface-to-volume and synergistic effect [221]. Once heterointerface forms, Fermi level-mediated charge transfer and band bending occur, usually resulting in a higher sensitivity. According to the types of participating semiconductors, Ga_2O_3 heterostructures can be divided into the n–n heterojunction and p–n heterojunction. Figure 14 illustrates the schematic diagram of the energy band structures for such kinds of heterojunctions. Many heterostructures, including heterojunctions and hierarchical heterostructures, have been developed by many researchers to improve the performance of Ga_2O_3 sensors. In the early years, Fleischer et al. [79,81,96,190] discovered a dramatic influence on the sensitivity and selectivity of Ga_2O_3 thin film sensors by sputtering different metal oxide, i.e., WO_3, Ta_2O_5, NiO, $AlVO_4$, CeO_2, Sm_2O_3, RhO, RuO, Ir_2O_3, and In_2O_3, as the surface modification layer. These types of thin film sensors could be employed as selective oxygen sensors for gas atmospheres with an overall excess of oxygen.

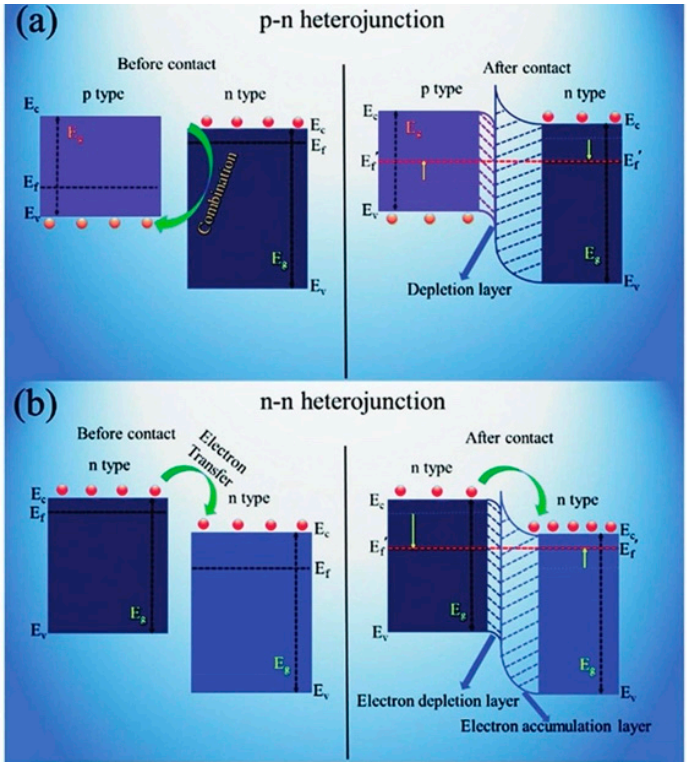

Figure 14. Schematic illustrations of the energy band structures at heterojunction interfaces of (**a**) p–n and (**b**) n–n of heterojunctions [178]. 2019 The Royal Society of Chemistry.

As for resistor-type of gas sensors, TiO_2, SnO_2, ZnO, WO_3, GaN, and GaS were used for constructing n–n heterostructures with Ga_2O_3 while NiO, CuO, LSFO, and LSCO of perovskite crystal structure for p–n heterostructures. Mohammadi and Fray [143] reported that mesoporous Ga_2O_3/TiO_2 thin film gas sensors had response values of 13.7 and 4.3 to 400 ppm CO and 10 ppm NO_2 gas at 200 °C, approximately 55% larger than pure TiO_2 sensors. Jang et al. [117], Liu et al. [139], and Abdullah et al. [132] studied the sensing

properties of Ga_2O_3/SnO_2 core–shell nanowires and nanobelts. Compared with pure Ga_2O_3 nanowire sensor, the optimum sensing temperature was reduced by 200 °C for Ga_2O_3/SnO_2 core–shell nanowire sensors that showed the highest ethanol response at 400 °C. Due to the fast physisorption of water and the fast formation of depletion layers caused by the large surface area of the amorphous SnO_2 shell and Ga_2O_3/SnO_2 heterojunction, Ga_2O_3/SnO_2 core–shell nanoribbons had a very high sensitivity to humidity with quick response and recovery near room temperature. At 25 °C, the conductivity of this nanoribbon humidity sensor at 75% relative humidity was three orders of magnitude larger than that at 5% relative humidity. The response time and recovery time were approximately 28 s and 7 s, respectively, when the relative humidity was switched between 5 and 75%. The H_2 gas sensor based on Ga_2O_3/SnO_2 core–shell nanobelts exhibited significant enhanced performance at room temperature in terms of response, response/recovery time and repeatability. During the exposure of 100 ppm NO_2, multiple networked Ga_2O_3/ZnO core–shell nanorod sensors showed a super response of 32.778% at 300 °C, which was 692 and 1791 times larger than that of bare Ga_2O_3 and bare ZnO nanorod sensors [126]. The sensor made by a wafer-scale ultra-thin Ga_2O_3/WO_3 heterostructure [168] exhibited about 4- and 10-fold improvement in the response to C_2H_6O compared to that of pure WO_3 and Ga_2O_3 nanofilm sensors at 275 °C. Furthermore, the Ga_2O_3/WO_3 heterostructural sensor possessed a shorter response/recover time and excellent selectivity. Park et al. [129] developed a Ga_2O_3/GaN core–shell nanowire sensor by surface-nitridated Ga_2O_3 nanowire. It showed responses of 160–363% to CO concentrations of 10–200 ppm at 150 °C, which were 1.6–3.1-fold greater than those of pristine Ga_2O_3 nanowire sensors.

For n–n junction, an accumulation layer is usually created, whereas a depletion layer forms in p–n junction. Lin et al. [154] and Zhang et al. [161] fabricated p–n heterostructural gas sensors using perovskite-sensitized Ga_2O_3 nanorod arrays for CO and NO_2 detection at high temperature. Figure 15 gives the TEM images and measured sensing performances of gas sensors made by $Ga_2O_3/La_{0.8}Sr_{0.2}FeO_3$ (LSFO) and $Ga_2O_3/La_{0.8}Sr_{0.2}CoO_3$ (LSCO) nanorods. Compared with the pristine Ga_2O_3 nanorod array sensor, close to 10 times enhanced sensitivity to 100 ppm CO was discovered for Ga_2O_3/LSFO sensors at 500 °C. In addition to the excellent CO sensitivity, the sensor based on Ga_2O_3/LSFO p–n heterostructure has a faster response time than that of the pristine Ga_2O_3 sensor. Ga_2O_3/LSCO sensors also showed nearly an order of magnitude enhanced sensitivity to 200 ppm NO_2 at 800 °C, along with much shorter response time. Ga_2O_3/CuO thin films were magnetron sputtered by Dyndal et al. [204] as a gas-sensitive material for C_3H_6O detection measured at 300 °C. Benefited from p–n heterostructure, Ga_2O_3/CuO thin film sensor exhibited 40% faster response time in comparison with pure CuO one. Sprincean et al. [134] made a Ga_2O_3/GaS:Zn nanostructured room temperature humidity sensor, which demonstrated acceptable sensitivity on the air relative humidity in the range from 42 to 92% and stable static characteristics over 6 months.

Additionally, Wang et al. [160] investigated the gas-sensing behavior of Ga_2O_3/Al_2O_3 nanocomposite and found that the composite-based sensor had a 6.5 times higher response to 100 ppm NO_x than that of the pure Ga_2O_3 sensor at room temperature. Notably, Sivasankaran and Balaji [177] synthesized mesoporous Ga_2O_3/reduced graphene oxide (rGO) nanocomposites by hydrothermal method. The results indicated that the sensing response to 200 ppm NH_3 of Ga_2O_3/rGO nanocomposite was 3.7-fold larger than that of pure Ga_2O_3 at room temperature.

As known, Ga_2O_3-based Shottky diode H_2 sensors generally has the MIS-type heterostructure in which β-Ga_2O_3 is served as reactive insulator and SiC [146], GaN [172,174], and AlGaN [173] are chosen as semiconductors. Lee et al. [174] concluded that the MIS-type sensor diodes exhibited better forward response than the MS-type Schottky sensor diode, because the β-Ga_2O_3 insulator surface provided more trap sites for hydrogen atoms at the metal–insulator interface.

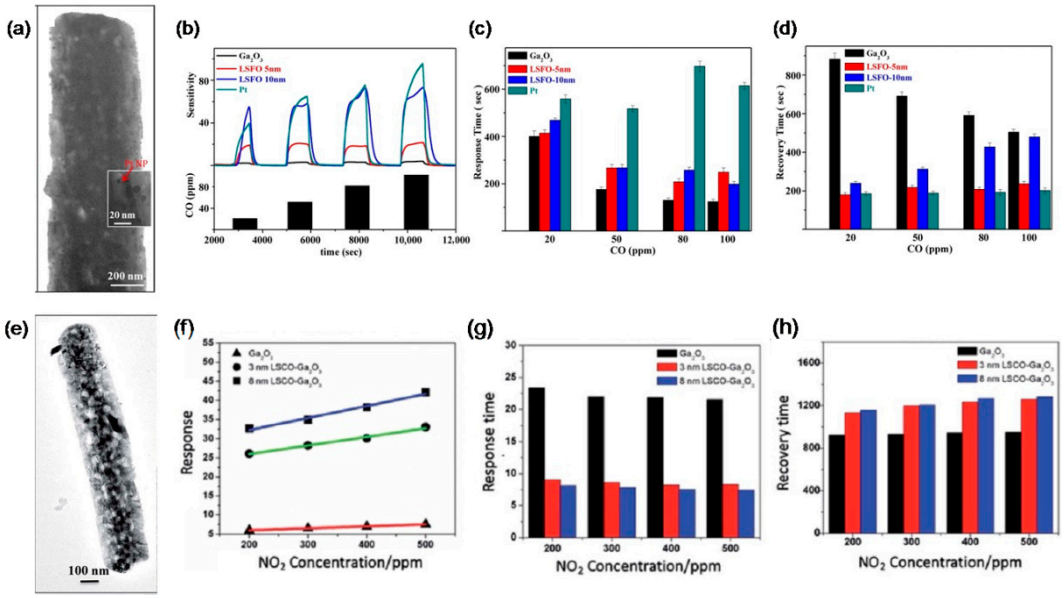

Figure 15. (**a**) TEM image of a β-Ga_2O_3 nanorod coated with 5 nm LSFO. (**b**) Sensitivity, (**c**) response time, and (**d**) recover time of gas sensors made by β-Ga_2O_3/LSFO nanorods upon exposure to CO at 500 °C [154]. Copyright 2016 American Chemical Society. (**e**) TEM image of a β-Ga_2O_3 nanorod coated with 8 nm LSCO. (**f**) Sensitivity, (**g**) response time, and (**h**) recover time of gas sensors made by β-Ga_2O_3/LSCO nanorods upon exposure to NO_2 at 800 °C [161]. Copyright 2020 The Royal Society of Chemistry.

5.4.5. Ga-Contained Metal Oxide

Aside from doping in Ga_2O_3, the gas-sensing properties can be optimized by intentional doping Ga^{3+} or solubility of Ga_2O_3 into other metal oxides. In general, host metal oxides are In_2O_3 [141,156,163–167,222], SnO_2 [223–225], and ZnO [145,226–229] for resistor gas sensors. Gas sensitive properties of Ga-doped In_2O_3 thin films and nanostructures were studied by Ratko et al. [222], Chen et al. [156], and Demin et al. [163–167]. Ga_2O_3 caused the formation of a porous or nanostructure in the In_2O_3-based ceramics, providing an active surface for reducing gases such as CH_4 [222] and CH_2O [156]. The response toward 100 ppm CH_2O of $Ga_xIn_{2-x}O_3$ nanofiber was about four times higher than that of pure In_2O_3. Meanwhile, it has superior ability to selectively detect CH_2O against other interfering VOCs. Demin et al. [163,164] obtained a high selectivity to NH_3 against C_2H_6O, C_3H_6O and liquefied petroleum gas based on 50% In_2O_3-50% Ga_2O_3 thin film-sensitive layer. The sensitivities towards O_2, CO, C_2H_6O, and CH_2O of Ga-doped SnO_2 materials were investigated by Silver et al. [223], Bagheri et al. [224], and Du et al. [225]. The Ga-doped SnO_2 thin film O_2 sensor showed sensitivity up to 2.1 for a partial pressure of oxygen as low as 1 Torr [223]. Bagheri et al. [224] observed the highest responses of 315 and 119 for 300 ppm CO and C_2H_6O by the SnO_2 sensors containing 5 and 1 wt% Ga_2O_3, respectively. With adding more than 25 wt% Ga_2O_3, the sensors became selective to CO and showed negligible responses to C_2H_6O and CH_4. The sensitivity to 50 ppm CH_2O of Ga-doped SnO_2 sensor was 4.5 times greater than that of the pure SnO_2 sensor. Moreover, it exhibited a lower detection limit of 0.1 ppm CH_2O with sensitivity of 3 and a short response-recovery time (3/39 s) and good selectivity. Ga-doped ZnO nanocrystalline film sensors were explored for detecting C_2H_6O, H_2S, NO_2, and H_2. The results demonstrated that the gas response of Ga-doped ZnO sensors were greatly enhanced by compared to pristine ZnO sensor. For instance, Hou et al. [145] observed a 60% enhancement of sensing response to H_2 by optimizing Ga composition to 0.3 at% compared with undoped ZnO sensors when measured at 130 °C. Moreover, the 0.3 at% Ga-doped ZnO sensor had a shorter response time and a better selectivity to H_2 in a mixture of H_2, CH_4, and NH_3. Rashid et al. [228] developed a 3%-Ga modified ZnO H_2 sensor whose resistive response

was improved six-fold compared with the pristine one at room temperature. It had a very low detection limit of 0.2 ppm. The enhanced H_2S-sensing properties of Ga-doped ZnO sensors were measured by Vorobyeva et al. [227] and by Girija et al. [229]. Figure 16 shows the H_2S response of Ga-doped ZnO gas sensors as functions of the gas concentration and temperature. In the presence of H_2S, chemisorbed oxygen interacts with the target gas as governed by the following reaction: $H_2S + 3O^- \rightarrow SO_2$ (g) + H_2O (g) + 3e. The enhanced sensitivity could be attributed to both excess of oxygen vacancies due to Ga^{3+} substitution and large adsorption energy of Ga for H_2S. Based on the liquid metal-based probe sonication route, Shafiei et al. [175] developed a quaternary $GaInSnO_x$ sensor and detection limits as low as 1 ppm and 20 ppm for NO_2 and NH_3 were obtained when operated at 100 °C. Table 4 summarizes the enhanced sensing performance of gas sensors using Ga-contained metal oxides toward different target gases for comparison.

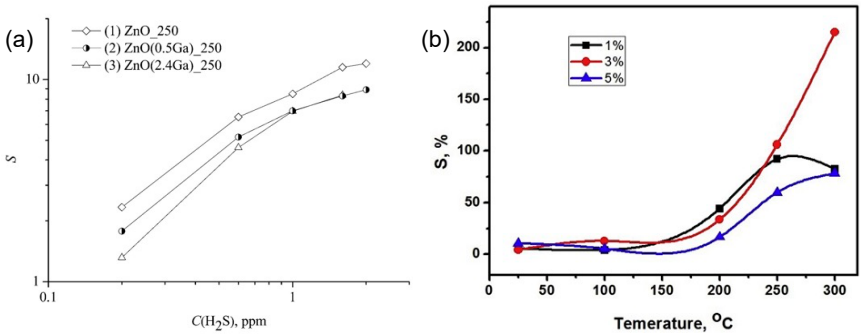

Figure 16. (**a**) H_2S Response of Ga-doped ZnO gas sensors as a function of the gas concentration [227]. Copyright 2013 Elsevier. (**b**) H_2S Response of Ga-doped ZnO gas sensors as a function of the temperature [229]. Copyright 2018 Elsevier.

5.4.6. Coating with Gas Filter

If working at high temperature, Ga_2O_3-based gas sensors (particularly resistor-type ones), similar to other metal oxide semiconductor sensors, suffer from an issue of poor selective gas detection, since they almost react to all reducing or oxidizing gases. One of the most efficient ways to improve the selectivity of gas sensors is the use of filters [182,230]. These filters, including physical and chemical filters, are highly permeable to the target gases and can hinder interfering gases from reaching the sensors surface. Figure 17 depicts the conceptual diagrams for physical and chemical filters of Ga_2O_3-based gas sensors. Fleischer et al. [95] designed a selective H_2 sensor by covering a SiO_2 physical gas-filtering layer on the Ga_2O_3 sputtered film for the first time. It was found that sensors with this surface layer structure had an extremely high specificity for H_2 upon exposure to a variety of interfering gases such as CO, CO_2, CH_4, C_4H_8, C_2H_6O, C_3H_6O, NO, and NH_3 at 700 °C. In another work of selective H_2, CH_4 and NO_x sensors operating at high temperature, Fleischer et al. [78] summarized that the SiO_2 physical filter can only permeate hydrogen and the porous Ga_2O_3 catalytic filter removes disturbing solvent vapors by oxidation, and the gas conversion filter composed of Pt supported on Al_2O_3 ensures a defined NO/NO_2 equilibrium. Flingelli et al. [77] fabricated a thin-film Ga_2O_3–gas sensor equipped with a screen printed porous Ga_2O_3 layer as catalytic filter for the selective detection of CH_4 even in the presence of C_2H_6O. It was observed that the cross-sensitivities eliminated for the organic solvents were oxidized while passing the filter, and only the quite stable methane was allowed to reach the sensor surface. Weh et al. [193,194] studied the optimization of physical filters for selective high-temperature H_2 sensors. A single SiO_2 filter, Ga_2O_3/SiO_2 and Al_2O_3/SiO_2 dual filter systems, and buried filter systems in which Ga_2O_3 or Cr-doped $SrTiO_3$ was buried between two SiO_2 layers were applied to improve the selectivity. The results indicated that optimizing filter systems could not only increase the selectivity but also the sensitivity of a given sensor. Furthermore, these filters can be additionally used to ensure the stability over the needed lifetime of the sensor.

Table 4. Enhanced sensing performances of gas sensors using Ga-contained metal oxides.

Sensing Material	Preparation	Sensitivity @Gas Concentration	Operating Temperature	Response/Recover Time (s)	Other Observations	Reference
Ga-doped In_2O_3 nanowire	CVD	$^{\triangle}$1.05 @ 80 ppm C_2H_6O	200	40/800		[141]
		$^{\triangle}$2.2 @ 4 ppm NO_2	200	1980/2780		
Ga-doped In_2O_3 nanofiber	Hydrothermal synthesis	$^{\Diamond}$52.5 @ 100 ppm CH_2O	150	1/70	The low limit of detection is 0.2 ppm	[156]
Ga-doped In_2O_3 film	PLD	$^{\square}$2.15 @ 25 ppm NH_3	623			[164]
		$^{\square}$20.5 @ 25 ppm C_2H_6O	504			
		$^{\square}$24.4 @ 25 ppm C_3H_6O	504			
		$^{\square}$7.47 @ 25 ppm CH_4	500			[167]
Ga-doped In_2O_3 ceramics	Coprecipitation	$^{\triangle}$0.85 @ 0.5% CH_4	380			[222]
Ga-doped SnO_2 film	Spray pyrolysis	$^{\Diamond}$3.1 @ 1 Torr O_2	350			[223]
Ga-doped SnO_2 nanocomposites	Coprecipitation	$^{\Diamond}$315 @ 300 ppm CO	300	36		[224]
Ga-doped SnO_2 nanocomposites		$^{\Diamond}$119 @ 300 ppm C_2H_6O	250	93		
Ga-doped SnO_2 microflowers	Hydrothermal synthesis	$^{\Diamond}$95.8 @ 50 ppm CH_2O	230	3	The low limit of detection is 0.1 ppm	[225]
Ga-doped ZnO film	Sol–gel synthesis	$^{\triangle}$0.5 @ 500 ppm H_2	130	475		[145]
Ga-doped ZnO Nanorod	Hydrothermal synthesis	$^{\triangle}$1.01% @ 250 ppm C_2H_6O	RT			[226]
Ga-doped ZnO nanoparticle	Spray pyrolysis	$^{\triangle}$56 @ 2 ppm NO_2	250			[227]
		$^{\triangle}$8 @ 1 ppm H_2S	250			
Ga-doped ZnO nanorod	Sol–gel synthesis	$^{\triangle}$0.91 @ 100 ppm H_2	RT	20		[228]
Ga-doped ZnO film	Magnetron sputtering	$^{\triangle}$2.4 @ 5 ppm H_2S	300			[229]

$^{\triangle}$ $S = (Ra - Rg)/Ra$; $^{\Diamond}$ $S = Ra/Rg$; $^{\square}$ $S = (Ra - Rg)/Rg$

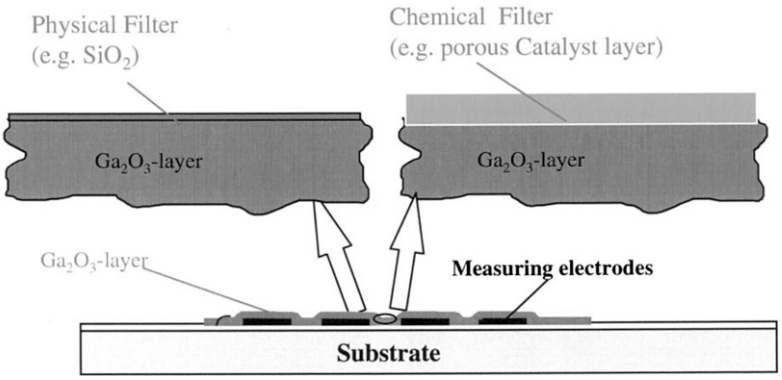

Figure 17. Conceptual diagrams for physical and chemical filters of Ga_2O_3-based gas sensors [230]. Copyright 1998 Elsevier.

5.4.7. Light Illumination

Light illumination rather than thermal activation is a promising strategy to enhance the gas-sensing of Ga_2O_3-based sensors. For clarity, the schematics and energy-level representations of the β-Ga_2O_3 nanowires before and after the 254 nm UV illumination are shown in Figure 18. When the sensors are illuminated under UV light with the photon energy equal or higher than the band gap of Ga_2O_3, electrons from the valence band can be rapidly excited to the conduction band, causing the desorption of oxygen from Ga_2O_3 surface and inducing the photosensitizing effect. Feng et al. [107] first reported a very fast room temperature oxygen response of the individual β-Ga_2O_3 nanowires synthesized by CVD under 254 nm UV illumination. This UV light-activated fast room temperature oxygen-

sensing characteristic was demonstrated in the thermal evaporated β-Ga_2O_3 nanobelts by Ma and Fan [112]. Juan et al. [130] studied the effect on the humidity-sensing properties of a β-Ga2O3 nanowire sensor from UV light. However, they found that the humidity sensitivity with UV illumination was lower than that in the dark, since the water molecules captured the electrons and holes generated by UV light in an environment with high relative humidity. Lin et al. [155] compared the effect of UV radiation on the CO sensors made by pure Ga_2O_3 nanorod arrays, Pt-decorated Ga_2O_3 nanorod arrays, and LSFO/Ga_2O_3 nanorod arrays. The measured results are shown in Figure 19a,b. Under 254 nm UV illumination, the sensitivity to 100 ppm CO was enhanced by about 30%, 20%, and 50% for pristine β-Ga_2O_3 nanorod arrays sensors, LSFO/Ga_2O_3 nanorod arrays sensors and Pt decorated Ga_2O_3 nanorod array sensors at 500 °C, respectively. Additionally, the response times were reduced for all cases, and up to 30% reduction of response time was achieved for LSFO/Ga_2O_3 nanorod arrays sensors. An et al. [128] showed a significant enhancement in the response of the Pt-functionalized Ga_2O_3 nanorods to NO_2 gas by UV irradiation at room temperature. It can be clearly seen from Figure 19c that the response to 5 ppm NO_2 increases from 175% to 931% with increasing the UV light illumination intensity from 0.35 to 1.2 mW/cm^2. A combination of the spillover effect and the enhancement of chemisorption and dissociation of gas results in the enhanced electrical response of the Pt-functionalized Ga_2O_3 nanostructured sensors. Sui et al. [64] realized the room temperature ozone sensing capability of InGaZnO (IGZO)-decorated amorphous Ga_2O_3 films under UV illumination.

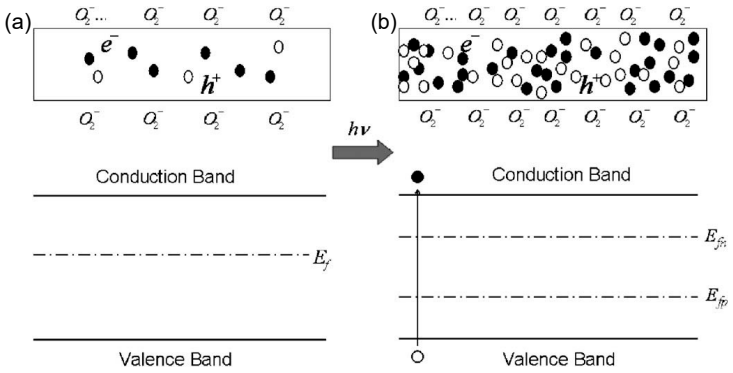

Figure 18. Schematics and energy-level representations of the β-Ga_2O_3 nanowires (**a**) before and (**b**) after the 254 nm UV illumination [107]. Copyright 2006 American Institute of Physics.

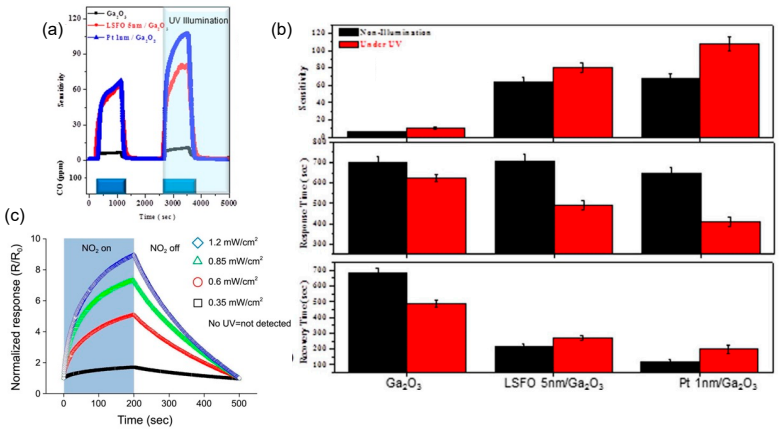

Figure 19. CO gas-sensing performance comparison of pristine, LSFO-decorated, and Pt-decorated β-Ga_2O_3 nanorod arrays: (**a**) normalized sensitivity time characteristics and (**b**) sensitivity, recovery time, and recovery time under dark or UV illumination tested at 500 °C [155]. Copyright 2017 American Institute of Physics. (**c**) Room temperature gas responses of Pt-functionalized Ga_2O_3 nanorod gas sensors to 5 ppm NO_2 under UV light illumination with varied intensities [128]. Copyright 2013 Korean Chemical Society.

6. Conclusions and Outlook

In conclusion, the past thirty years have witnessed very impressive progress in the field of Ga_2O_3-based gas sensors. It has been proven that β-Ga_2O_3 polycrystalline thin films and nanostructures have great potential in detecting oxygen and many reducing gases in a wide temperature range from room temperature to 1000 °C. Some growth techniques with low cost, simple process, and flexible operation are available to prepare Ga_2O_3-sensing material. Compared with the gas sensors made by other metal oxides such as SnO_2, Ga_2O_3-based gas sensors have the advantages of long-term stability, fast response and recovery times, good reproducibility, low cross-sensitivity to water vapor, and short preaging time [181]. Figure 20 displays the radar chart of seven performance enhancement strategies of gas sensors made by Ga_2O_3 bulk crystal, thin films, and nanostructures. Although the performance of Ga_2O_3-based gas sensors has been improved through various enhancement strategies, from a practical point of view, continuous efforts should be made to further increase the gas selectivity, to decrease the operating temperature, and to develop high-speed nonresistive types of sensors. In-depth understanding of the interaction between the target gas and Ga_2O_3 surface, as well as the gas-sensing behavior, are also needed using newly developed computational tools. Some suggestions on future research opportunities of Ga_2O_3-based gas sensors are listed below:

(i) Construction of hybrid structures with two-dimensional (2D) materials and organic polymers. Two-dimensional materials are regarded as having promising potential for gas-sensing devices owing to their large surface-to-volume ratio and high surface sensitivity [231]. The integration of 2D layers with Ga_2O_3, especially a 2D Ga_2O_3 monolayer [232], can form a van der Waals heterojunction without constraints on the chemical bonding and interfacial lattice matching, which will be expected to widen the building blocks for novel applications with unprecedented properties and excellent performance. The energy band alignment of such van der Waals heterojunction could be precisely designed by selecting suitable 2D materials, such as transition metal dichalcogenides with different band gaps and working functions so as to optimize the gas selectivity and performance of the Ga_2O_3 gas sensor. Additionally, organic semiconductors offer a viable alternative to conventional inorganic semiconductors in gas sensor applications because of their unusual electrical properties, diversity, large area, and potentially low cost [233]. They show good sensitivities toward many gases or vapors, ranging from organic solvents to inorganic gases. Moreover, it allows for the inexpensive fabrication of novel Ga_2O_3 gas sensors using organic polymers as a platform, owing to their porosity, mechanical flexibility, environmental stability, and solution processability. Therefore, more research should be conducted to fabricate Ga_2O_3-based gas sensors by constructing heterostructures with 2D materials and organic polymers, which may result in some novel features and potential applications.

(ii) Combinations with DFT calculations and machine learning. Hitherto, quite few theoretical investigations have been devoted to understanding the interaction behaviors between gas molecules and Ga_2O_3 in the field of gas sensors. DFT calculations [232,234,235] have been performed to study the adsorption, dissociation, and diffusion characteristics of gas molecules on the surface of Ga_2O_3. It is suggested that the calculated adsorption energy, electron structures of oxygen vacancy, and charge transfer are highly significant in defining the performance of a sensor. Large adsorption energy and significant charge transfer indicate high sensitivity and selectivity towards a specific gas. Alongside DFT, machine learning is considered as an effective data processing approach for developing smart devices with the ability to deal with selectivity and drift problems [236]. The machine learning technique involves data processing of sensor output, dimensionality reduction, and then training a system/network for the predictions. Therefore, DFT and machine learning can be implemented as a powerful tool for studying gas-sensing behavior and provide valuable suggestions and predictions of gas-sensing materials and target gas species.

(iii) Development of optical sensors. Compared to electrical characteristic gas sensors, more attention should be paid on the less-explored sensors using the promising optical properties of Ga_2O_3. In a pioneer study on Ga_2O_3-based optical gas sensors, Reiprich et al. [122] pointed out that the spectral composition of photoluminescence showed a strong intensity difference upon exposure to various gases at room temperature indirectly caused by the negatively charged oxygen ions in Ga_2O_3. Optical gas sensors offer a number of advantages, such as fast responses, minimal drift and high gas specificity [187]. Gas detection can be made in real time and in situ by adopting optical sensors. With the help of the rapid developed technology of Ga_2O_3 optical devices, it is possible to design Ga_2O_3-based optical gas sensors that can measure gas concentrations in the ppm or ppb range with zero cross-response to other gases and high temporal resolution. In this way, optical gas-sensing fills a gap between low-cost electrical/electrochemical sensors with inferior performance and high-end analytic equipment.

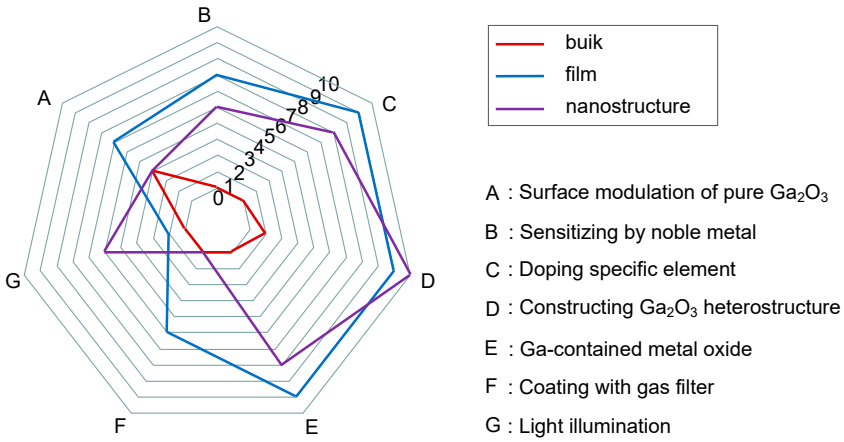

Figure 20. Radar chart of seven performance enhancement strategies of gas sensors made by Ga_2O_3 bulk crystal, thin films, and nanostructures. Original drawing was done by us.

Moreover, the researchers should explore the options for the use of Ga_2O_3 in many other sensor applications such as chemical sensors [237,238] and biosensors [239,240] to detect metal ions, e.g., Ni^{2+} and Fe^{2+}, and DNA sequences in biological fluids, tap water, and so forth. It is believed that Ga_2O_3 will play a significant role in the field of safety, environmental, and medical monitoring systems with the development of device designs and fabrication technologies.

Funding: This work was supported by the National Natural Science Foundation of China (Grant Nos. 12164031, 11864029, 62004078, 12105033, 11774235, and 11933005); National Key R&D Program of China (Grant No. 2022YFE0107400); Natural Science Foundation of Inner Mongolia Autonomous Region of China (Grant Nos. 2020MS01014 and 2020MS06007); the Fundamental Research Funds for the Central Universities (Grant No. DUT20RC(3)042); and the Program for Professor of Special Appointment (Eastern Scholar) at Shanghai Institutions of Higher Learning (GZ2020015).

Acknowledgments: Jun Zhu gratefully acknowledges Xue-Lun Wang for meaning discussions when visiting National Institute of Advanced Industrial Science and Technology (AIST) in Japan.

Conflicts of Interest: The authors declare no conflict of interest.

References

1. Tsao, J.Y.; Chowdhury, S.; Hollis, M.A.; Jena, D.; Johnson, N.M.; Jones, K.A.; Kaplar, R.J.; Rajan, S.; Van de Walle, C.G.; Bellotti, E.; et al. Ultrawide-bandgap semiconductors: Research opportunities and challenges. *Adv. Electron. Mater.* **2018**, *4*, 1600501. [CrossRef]
2. Higashiwaki, M.; Sasaki, K.; Kuramata, A.; Masui, T.; Yamakoshi, S. Gallium oxide (Ga_2O_3) metal-semiconductor field-effect transistors on single-crystal β-Ga_2O_3 (010) substrates. *Appl. Phys. Lett.* **2012**, *100*, 013504. [CrossRef]

3. Pearton, S.; Ren, F.; Mastro, M. *Gallium Oxide: Technology, Devices and Applications*; Elsevier: Amsterdam, The Netherlands, 2019; pp. 439–464. [CrossRef]
4. Higashiwaki, M.; Fujita, S. *Gallium Oxide: Materials Properties, Crystal Growth, and Devices*; Springer Nature: Cham, Switzerland, 2020; pp. 1–11. [CrossRef]
5. Xue, H.; He, Q.; Jian, G.; Long, S.; Pang, T.; Liu, M. An overview of the ultrawide bandgap Ga_2O_3 semiconductor-based Schottky barrier diode for power electronics application. *Nanoscale Res. Lett.* **2018**, *13*, 290. [CrossRef]
6. Liu, Z.; Li, P.; Zhi, Y.; Wang, X.; Chu, X.; Tang, W. Review of gallium oxide based field-effect transistors and Schottky barrier diodes. *Chin. Phys. B* **2019**, *28*, 017105. [CrossRef]
7. Dong, H.; Xue, H.; He, Q.; Qin, Y.; Jian, G.; Long, S.; Liu, M. Progress of power field effect transistor based on ultra-wide bandgap Ga_2O_3 semiconductor material. *J. Semicond.* **2019**, *40*, 011802. [CrossRef]
8. Zhang, H.; Yuan, L.; Tang, X.; Hu, J.; Sun, J.; Zhang, Y.; Zhang, Y. Progress of ultra-wide bandgap Ga_2O_3 semiconductor materials in power MOSFETs. *IEEE Trans. Power Electron.* **2020**, *35*, 5157–5179. [CrossRef]
9. Singh, R.; Lenka, T.R.; Panda, D.K.; Velpula, R.T.; Jain, B.; Bui, H.Q.T.; Nguyen, H.P.T. The dawn of Ga_2O_3 HEMTs for high power electronics—A review. *Mater. Sci. Semicond. Process.* **2020**, *119*, 105216. [CrossRef]
10. Wong, M.H.; Higashiwaki, M. Vertical β-Ga_2O_3 power transistors: A review. *IEEE Trans. Electron Dev.* **2020**, *67*, 3925–3937. [CrossRef]
11. Kumar, S.; Singh, R. Nanofunctional gallium oxide (Ga_2O_3) nanowires/nanostructures and their applications in nanodevices. *Phys. Status Solidi RRL* **2013**, *7*, 781–792. [CrossRef]
12. Higashiwaki, M.; Sasaki, K.; Murakami, H.; Kumagai, Y.; Koukitu, A.; Kuramata, A.; Masui, T.; Yamakoshi, S. Recent progress in Ga_2O_3 power devices. *Semicond. Sci. Technol.* **2016**, *31*, 034001. [CrossRef]
13. Mastro, M.A.; Kuramata, A.; Calkins, J.; Kim, J.; Ren, F.; Pearton, S.J. Opportunities and future directions for Ga_2O_3. *ECS J. Solid State Sci. Technol.* **2017**, *6*, P356–P359. [CrossRef]
14. Pearton, S.J.; Yang, J.; Cary IV, P.H.; Ren, F.; Kim, J.; Tadjer, M.J.; Mastro, M.A. A review of Ga_2O_3 materials, processing, and devices. *Appl. Phys. Rev.* **2018**, *5*, 011301. [CrossRef]
15. Galazka, Z. β-Ga_2O_3 for wide-bandgap electronics and optoelectronics. *Semicond. Sci. Technol.* **2018**, *33*, 113001. [CrossRef]
16. Baldini, M.; Galazka, Z.; Wagner, G. Recent progress in the growth of β-Ga_2O_3 for power electronics applications. *Mater. Sci. Semicond. Process.* **2018**, *78*, 132–146. [CrossRef]
17. Higashiwaki, M.; Jessen, G.H. The dawn of gallium oxide microelectronics. *Appl. Phys. Lett.* **2018**, *112*, 060401. [CrossRef]
18. Zhou, H.; Zhang, J.; Zhang, C.; Feng, Q.; Zhao, S.; Ma, P.; Hao, Y. A review of the most recent progresses of state-of-art gallium oxide power devices. *J. Semicond.* **2019**, *40*, 011803. [CrossRef]
19. Xu, J.; Zheng, W.; Huang, F. Gallium oxide solar-blind ultraviolet photodetectors: A review. *J. Mater. Chem. C* **2019**, *7*, 8753–8770. [CrossRef]
20. Kim, J.; Pearton, S.J.; Fares, C.; Yang, J.; Ren, F.; Kim, S.; Polyakov, A.Y. Radiation damage effects in Ga_2O_3 materials and devices. *J. Mater. Chem. C* **2019**, *7*, 10–24. [CrossRef]
21. Qin, Y.; Long, S.; Dong, H.; He, Q.; Jian, G.; Zhang, Y.; Hou, X.; Tan, P.; Zhang, Z.; Lv, H.; et al. Review of deep ultraviolet photodetector based on gallium oxide. *Chin. Phys. B* **2019**, *28*, 018501. [CrossRef]
22. Guo, D.; Guo, Q.; Chen, Z.; Wu, Z.; Li, P.; Tang, W. Review of Ga_2O_3-based optoelectronic devices. *Mater. Today Phys.* **2019**, *11*, 100157. [CrossRef]
23. Chen, X.; Ren, F.; Gu, S.; Ye, J. Review of gallium-oxide-based solar-blind ultraviolet photodetectors. *Photonics Res.* **2019**, *7*, 381. [CrossRef]
24. Saikumar, A.K.; Nehate, S.D.; Sundaram, K.B. Review-RF sputtered films of Ga_2O_3. *ECS J. Solid State Sci. Technol.* **2019**, *8*, Q3064–Q3078. [CrossRef]
25. Tadjer, M.J.; Lyons, J.L.; Nepal, N.; Freitas, J.A., Jr.; Koehler, A.D.; Foster, G.M. Review-theory and characterization of doping and defects in β-Ga_2O_3. *ECS J. Solid State Sci. Technol.* **2019**, *8*, Q3187–Q3194. [CrossRef]
26. Afzal, A. β-Ga_2O_3 nanowires and thin films for metal oxide semiconductor gas sensors: Sensing mechanisms and performance enhancement strategies. *J. Mater.* **2019**, *5*, 542–557. [CrossRef]
27. Zhai, H.; Wu, Z.; Fang, Z. Recent progress of Ga_2O_3-based gas sensors. *Ceram. Int.* **2022**, *48*, 24213–24233. [CrossRef]
28. McCluskey, M.D. Point defects in Ga_2O_3. *J. Appl. Phys.* **2020**, *127*, 101101. [CrossRef]
29. Zhang, J.; Shi, J.; Qi, D.; Chen, L.; Zhang, K.H.L. Recent progress on the electronic structure, defect, and doping properties of Ga_2O_3. *APL Mater.* **2020**, *8*, 020906. [CrossRef]
30. Bosi, M.; Mazzolini, P.; Seravalli, L.; Fornari, R. Ga_2O_3 polymorphs: Tailoring the epitaxial growth conditions. *J. Mater. Chem. C* **2020**, *8*, 10975–10992. [CrossRef]
31. Hou, X.; Zou, Y.; Ding, M.; Qin, Y.; Zhang, Z.; Ma, X.; Tan, P.; Yu, S.; Zhou, X.; Zhao, X.; et al. Review of polymorphous Ga_2O_3 materials and their solar-blind photodetector applications. *J. Phys. D Appl. Phys.* **2021**, *54*, 043001. [CrossRef]
32. Tak, B.R.; Kumar, S.; Kapoor, A.K.; Wang, D.; Li, X.; Sun, H.; Singh, R. Recent advances in the growth of gallium oxide thin films employing various growth techniques—A review. *J. Phys. D Appl. Phys.* **2021**, *54*, 453002. [CrossRef]
33. Blevins, J.; Yang, G. On optical properties and scintillation performance of emerging Ga_2O_3: Crystal growth, emission mechanisms and doping strategies. *Mater. Res. Bull.* **2021**, *144*, 111494. [CrossRef]

34. Yuan, Y.; Hao, W.; Mu, W.; Wang, Z.; Chen, X.; Liu, Q.; Xu, G.; Wang, C.; Zhou, H.; Zou, Y.; et al. Toward emerging gallium oxide semiconductors: A roadmap. *Fundam. Res.* **2021**, *1*, 697–716. [CrossRef]
35. Huang, H.-C.; Ren, Z.; Chan, C.; Li, X. Wet etch, dry etch, and MacEtch of β-Ga_2O_3: A review of characteristics and mechanism. *J. Mater. Res.* **2021**, *36*, 4756–4770. [CrossRef]
36. Galazka, Z.; Ganschow, S.; Irmscher, K.; Klimm, D.; Albrecht, M.; Schewski, R.; Pietsch, M.; Schulz, T.; Dittmar, A.; Kwasniewski, A.; et al. Bulk single crystals of β-Ga_2O_3 and Ga-based spinels as ultra-wide bandgap transparent semiconducting oxides. *Prog. Cryst. Growth Charact. Mater.* **2021**, *67*, 100511. [CrossRef]
37. Sharma, R.; Law, M.E.; Ren, F.; Polyakov, A.Y.; Pearton, S.J. Diffusion of dopants and impurities in β-Ga_2O_3. *J. Vac. Sci. Technol. A* **2021**, *39*, 060801. [CrossRef]
38. Cooke, J.; Sensale-Rodriguez, B.; Ghadbeigi, L. Methods for synthesizing β-Ga_2O_3 thin films beyond epitaxy. *J. Phys. Photonics* **2021**, *3*, 032005. [CrossRef]
39. Wang, C.; Zhang, J.; Xu, S.; Zhang, C.; Feng, Q.; Zhang, Y.; Ning, J.; Zhao, S.; Zhou, H.; Hao, Y. Progress in state-of-the-art technologies of Ga_2O_3 devices. *J. Phys. D Appl. Phys.* **2021**, *54*, 243001. [CrossRef]
40. Kim, H. Control and understanding of metal contacts to β-Ga_2O_3 single crystals: A review. *SN Appl. Sci.* **2022**, *4*, 27. [CrossRef]
41. Fleischer, M.; Meixner, H. Gallium oxide thin films: A new material for high-temperature oxygen sensors. *Sens. Actuators B Chem.* **1991**, *4*, 437–441. [CrossRef]
42. Fleischer, M.; Meixner, H. Oxygen sensing with long-term stable Ga_2O_3 thin films. *Sens. Actuators B Chem.* **1991**, *5*, 115–119. [CrossRef]
43. Malik, R.; Tomer, V.K.; Mishra, Y.K.; Lin, L. Functional gas sensing nanomaterials: A panoramic view. *Appl. Phys. Rev.* **2020**, *7*, 021301. [CrossRef]
44. Herbstein, F.H. Diversity amidst similarity: A multidisciplinary approach to phase relationships, solvates, and polymorphs. *Cryst. Growth Des.* **2004**, *4*, 1419–1429. [CrossRef]
45. Roy, R.; Hill, V.; Osborn, E. Polymorphism of Ga_2O_3 and the system Ga_2O_3-H_2O. *J. Am. Chem. Soc.* **1952**, *74*, 719–722. [CrossRef]
46. Yoshioka, S.; Hayashi, H.; Kuwabara, A.; Oba, F.; Matsunaga, K.; Tanaka, I. Structures and energetics of Ga_2O_3 polymorphs. *J. Phys. Condens. Matter* **2007**, *19*, 346211. [CrossRef]
47. Zinkevich, M.; Aldinger, F. Thermodynamic assessment of the gallium-oxygen system. *J. Am. Ceram. Soc.* **2004**, *87*, 683–691. [CrossRef]
48. Playford, H.Y.; Hannon, A.C.; Barney, E.R.; Walton, R.I. Structures of uncharacterised polymorphs of gallium oxide from total neutron diffraction. *Chem. Eur. J.* **2013**, *19*, 2803–2813. [CrossRef]
49. Cora, I.; Mezzadri, F.; Boschi, F.; Bosi, M.; Caplovicova, M.; Calestani, G.; Dodony, I.; Pecza, B.; Fornari, R. The real structure of ε-Ga_2O_3 and its relation to κ-phase. *CrystEngComm* **2017**, *19*, 1509–1516. [CrossRef]
50. Kim, J.; Tahara, D.; Miura, Y.; Kim, B.G. First-principle calculations of electronic structures and polar properties of (κ, ε)-Ga_2O_3. *Appl. Phys. Express* **2018**, *11*, 061101. [CrossRef]
51. Nishinaka, H.; Ueda, O.; Tahara, D.; Ito, Y.; Ikenaga, N.; Hasuike, N.; Yoshimoto, M. Single-domain and atomically flat surface of κ-Ga_2O_3 thin films on FZ-grown ε-$GaFeO_3$ substrates via step-flow growth mode. *ACS Omega* **2020**, *5*, 29585–29592. [CrossRef]
52. Jang, S.; Jung, S.; Kim, J.; Ren, F.; Pearton, S.J.; Baik, K.H. Hydrogen sensing characteristics of Pt Schottky diodes on ($\bar{2}$01) and (010) Ga_2O_3 single crystals. *ECS J. Solid State Sci. Technol.* **2018**, *7*, Q3180–Q3182. [CrossRef]
53. Fleischer, M.; Handrider, W.; Meixner, H. Stability of semiconducting gallium oxide thin films. *Thin Solid Films* **1990**, *190*, 93–102. [CrossRef]
54. Ueda, N.; Hosono, H.; Waseda, R.; Kawazoe, H. Synthesis and control of conductivity of ultraviolet transmitting β-Ga_2O_3 single crystals. *Appl. Phys. Lett.* **1997**, *70*, 3561–3563. [CrossRef]
55. Varley, J.B.; Weber, J.R.; Janotti, A.; Van de Walle, C.G. Oxygen vacancies and donor impurities in β-Ga_2O_3. *Appl. Phys. Lett.* **2010**, *97*, 142106. [CrossRef]
56. Feng, Z.; Bhuiyan, A.F.M.A.U.; Karim, M.R.; Zhao, H. MOCVD homoepitaxy of Si-doped (010) β-Ga_2O_3 thin films with superior transport properties. *Appl. Phys. Lett.* **2019**, *114*, 250601. [CrossRef]
57. Fleischer, M.; Meixner, H. Electron mobility in single and polycrystalline Ga_2O_3. *J. Appl. Phys.* **1993**, *74*, 300–305. [CrossRef]
58. Irmscher, K.; Galazka, Z.; Pietsch, M.; Uecker, R.; Fornari, R. Electrical properties of β-Ga_2O_3 single crystals grown by the Czochralski method. *J. Appl. Phys.* **2011**, *110*, 063720. [CrossRef]
59. Ma, N.; Tanen, N.; Verma, A.; Guo, Z.; Luo, T.; Xing, H.; Jena, D. Intrinsic electron mobility limits in β-Ga_2O_3. *Appl. Phys. Lett.* **2016**, *109*, 212101. [CrossRef]
60. Goto, K.; Konishi, K.; Murakami, H.; Kumagai, Y.; Monemar, B.; Higashiwaki, M.; Kuramata, A.; Yamakoshi, S. Halide vapor phase epitaxy of Si doped β-Ga_2O_3 and its electrical properties. *Thin Solid Films* **2018**, *666*, 182–184. [CrossRef]
61. Spencer, J.A.; Mock, A.L.; Jacobs, A.G.; Schubert, M.; Zhang, Y.; Tadjer, M.J. A review of band structure and material properties of transparent conducting and semiconducting oxides: Ga_2O_3, Al_2O_3, In_2O_3, ZnO, SnO_2, CdO, NiO, CuO, and Sc_2O_3. *Appl. Phys. Rev.* **2022**, *9*, 011315. [CrossRef]
62. Ogita, M.; Higo, K.; Nakanishi, Y.; Hatanaka, Y. Ga_2O_3 thin film for oxygen sensor at high temperature. *Appl. Surf. Sci.* **2001**, *175–176*, 721–725. [CrossRef]
63. Ogita, M.; Yuasa, S.; Kobayashi, K.; Yamada, Y.; Nakanishi, Y.; Hatanaka, Y. Presumption and improvement for gallium oxide thin film of high temperature oxygen sensors. *Appl. Surf. Sci.* **2003**, *212–213*, 397–401. [CrossRef]

64. Sui, Y.X.; Liang, H.L.; Chen, Q.S.; Huo, W.X.; Du, X.L.; Mei, Z.X. Room-temperature ozone sensing capability of IGZO-decorated amorphous Ga_2O_3 films. *ACS Appl. Mater. Interfaces* **2020**, *12*, 8929–8934. [CrossRef] [PubMed]
65. Almaev, A.V.; Nikolaev, V.I.; Stepanov, S.I.; Pechnikov, A.I.; Chernikov, E.V.; Davletkildeev, N.A.; Sokolov, D.V.; Yakovlev, N.N.; Kalygina, V.M.; Kopyev, V.V.; et al. Hydrogen influence on electrical properties of Pt-contacted α-Ga_2O_3/ε-Ga_2O_3 structures grown on patterned sapphire substrates. *J. Phys. D Appl. Phys.* **2020**, *53*, 414004. [CrossRef]
66. Almaev, A.; Nikolaev, V.; Butenko, P.; Stepanov, S.; Pechnikov, A.; Yakovlev, N.; Sinyugin, I.; Shapenkov, S.; Scheglov, M. Gas sensors based on pseudohexagonal phase of gallium oxide. *Phys. Status Solidi B* **2022**, *259*, 2100306. [CrossRef]
67. Bartic, M.; Baban, C.; Suzuki, H.; Ogita, M.; Isai, M. β-gallium oxide as oxygen gas sensors at a high temperature. *J. Am. Ceram. Soc.* **2007**, *90*, 2879–2884. [CrossRef]
68. Nakagomi, S.; Kaneko, M.; Kokubun, Y. Hydrogen sensitive Schottky diode based on β-Ga_2O_3 single crystal. *Sens. Lett.* **2011**, *9*, 31–35. [CrossRef]
69. Nakagomi, S.; Ikeda, M.; Kokubun, Y. Comparison of hydrogen sensing properties of Schottky diodes based on SiC and β-Ga_2O_3 single crystal. *Sens. Lett.* **2011**, *9*, 616–620. [CrossRef]
70. Bartic, M. Mechanism of oxygen sensing on β-Ga_2O_3 single-crystal sensors for high temperatures. *Phys. Status Solidi A* **2016**, *213*, 457–462. [CrossRef]
71. Uhlendorf, J.; Galazka, Z.; Schmidt, H. Oxygen diffusion in β-Ga_2O_3 single crystals at high temperatures. *Appl. Phys. Lett.* **2021**, *119*, 242106. [CrossRef]
72. Macri, P.P.; Enzo, S.; Sberveglieri, G.; Groppelli, S.; Perego, C. Unknown Ga_2O_3 structural phase and related characteristics as active layers for O_2 sensors. *Appl. Surf. Sci.* **1993**, *65–66*, 277–282. [CrossRef]
73. Fleischer, M.; Meixner, H. A selective CH_4 sensor using semiconducting Ga_2O_3 thin films based on temperature switching of multigas reactions. *Sens. Actuators B Chem.* **1995**, *25*, 544–547. [CrossRef]
74. Bausewein, A.; Hacker, B.; Fleischer, M.; Meixner, H. Effects of palladium dispersions on gas-sensitive conductivity of semiconducting Ga_2O_3 thin-film ceramics. *J. Am. Ceram. Soc.* **1997**, *80*, 317–323. [CrossRef]
75. Schwebel, T.; Fleischer, M.; Meixner, H.; Kohl, C.-D. CO-sensor for domestic use based on high temperature stable Ga_2O_3 thin films. *Sens. Actuators B Chem.* **1998**, *49*, 46–51. [CrossRef]
76. Josepovits, V.K.; Krafcsik, O.; Kiss, G.; Perczel, I.V. Effect of gas adsorption on the surface structure of β-Ga_2O_3 studied by XPS and conductivity measurements. *Sens. Actuators B Chem.* **1998**, *48*, 373–375. [CrossRef]
77. Flingelli, G.K.; Fleischer, M.; Meixner, H. Selective detection of methane in domestic environments using a catalyst sensor system based on Ga_2O_3. *Sens. Actuators B Chem.* **1998**, *48*, 258–262. [CrossRef]
78. Fleischer, M.; Kornely, S.; Weh, T.; Frank, J.; Meixner, H. Selective gas detection with high-temperature operated metal oxides using catalytic filters. *Sens. Actuators B Chem.* **2000**, *69*, 205–210. [CrossRef]
79. Lang, A.C.; Fleischer, M.; Meixner, H. Surface modifications of Ga_2O_3 thin film sensors with Rh, Ru and Ir clusters. *Sens. Actuators B Chem.* **2000**, *66*, 80–84. [CrossRef]
80. Bene, R.; Pinter, Z.; Perczel, I.V.; Fleischer, M.; Reti, F. High-temperature semiconductor gas sensors. *Vacuum* **2001**, *61*, 275–278. [CrossRef]
81. Frank, J.; Fleischer, M.; Zimmer, M.; Meixner, H. Ozone sensing using In_2O_3 modified Ga_2O_3 thin films. *IEEE Sens. J.* **2001**, *1*, 318–321. [CrossRef]
82. Frank, J.; Meixner, H. Sensor system for indoor air monitoring using semiconducting metal oxides and IR-absorption. *Sens. Actuators B Chem.* **2001**, *78*, 298–302. [CrossRef]
83. Kiss, G.; Pinter, Z.; Perczel, I.V.; Sassi, Z.; Reti, F. Study of oxide semiconductor sensor materials by selected methods. *Thin Solid Films* **2001**, *391*, 216–223. [CrossRef]
84. Lampe, U.; Simon, E.; Pohle, R.; Fleischer, M.; Meixner, H.; Frerichs, H.-P.; Lehmann, M.; Kiss, G. GasFET for the detection of reducing gases. *Sens. Actuators B Chem.* **2005**, *111–112*, 106–110. [CrossRef]
85. Stegmeier, S.; Fleischer, M.; Hauptmann, P. Influence of the morphology of platinum combined with β-Ga_2O_3 on the VOC response of work function type sensors. *Sens. Actuators B Chem.* **2010**, *148*, 439–449. [CrossRef]
86. Stegmeier, S.; Fleischer, M.; Hauptmann, P. Thermally activated platinum as VOC sensing material for work function type gas sensors. *Sens. Actuators B Chem.* **2010**, *144*, 418–424. [CrossRef]
87. Almaev, A.V.; Chernikov, E.V.; Davletkildeev, N.A.; Sokolov, D.V. Oxygen sensors based on gallium oxide thin films with addition of chromium. *Superlattices Microstruct.* **2020**, *139*, 106392. [CrossRef]
88. Almaev, A.V.; Chernikov, E.V.; Novikov, V.V.; Kushnarev, B.O.; Yakovlev, N.N.; Chuprakova, E.V.; Oleinik, V.L.; Lozinskaya, A.D.; Gogova, D.S. Impact of Cr_2O_3 additives on the gas-sensitive properties of β-Ga_2O_3 thin films to oxygen, hydrogen, carbon monoxide, and toluene vapors. *J. Vac. Sci. Technol. A* **2021**, *39*, 023405. [CrossRef]
89. Fleischer, M.; Giber, J.; Meixner, H. H_2-induced changes in electrical conductance of β-Ga_2O_3 thin-film systems. *Appl. Phys. A* **1992**, *54*, 560–566. [CrossRef]
90. Fleischer, M.; Meixner, H. Improvements in Ga_2O_3 sensors for reducing gases. *Sens. Actuators B Chem.* **1993**, *13*, 259–263. [CrossRef]
91. Fleischer, M.; Hollbauer, L.; Meixner, H. Effect of the sensor structure on the stability of Ga_2O_3 sensors for reducing gases. *Sens. Actuators B Chem.* **1994**, *18–19*, 119–124. [CrossRef]

92. Fleischer, M.; Meixner, H. In situ Hall measurements at temperatures up to 1100 degrees C with selectable gas atmospheres. *Meas. Sci. Technol.* **1994**, *5*, 580–583. [CrossRef]
93. Fleischer, M.; Wagner, V.; Hacker, B.; Meixner, H. Comparison of a.c. and d.c. measurement techniques using semiconducting Ga_2O_3 sensors. *Sens. Actuators B Chem.* **1995**, *26–27*, 85–88. [CrossRef]
94. Fleischer, M.; Meixner, H. Sensitive, selective and stable CH_4 detection using semiconducting Ga_2O_3 thin films. *Sens. Actuators B Chem.* **1995**, *26–27*, 81–84. [CrossRef]
95. Fleischer, M.; Seth, M.; Kohl, C.-D.; Meixner, H. A selective H_2 sensor implemented using Ga_2O_3 thin-films which are covered with a gas-filtering SiO_2 layer. *Sens. Actuators B Chem.* **1996**, *35–36*, 297–302. [CrossRef]
96. Fleischer, M.; Seth, M.; Koh, C.-D.; Meixner, H. A study of surface modification at semiconducting Ga_2O_3 thin film sensors for enhancement of the sensitivity and selectivity. *Sens. Actuators B Chem.* **1996**, *35–36*, 290–296. [CrossRef]
97. Reti, F.; Fleischer, M.; Perczel, I.V.; Meixner, H.; Giber, J. Detection of reducing gases in air by β-Ga_2O_3 thin films using self-heated and externally (oven-) heated operation modes. *Sens. Actuators B Chem.* **1996**, *34*, 378–382. [CrossRef]
98. Baban, C.-I.; Toyoda, Y.; Ogita, M. High temperature oxygen sensor using a Pt-Ga_2O_3-Pt sandwich structure. *Jpn. J. Appl. Phys.* **2004**, *43*, 7213–7216. [CrossRef]
99. Baban, C.; Toyoda, Y.; Ogita, M. Oxygen sensing at high temperatures using Ga_2O_3 films. *Thin Solid Films* **2005**, *484*, 369–373. [CrossRef]
100. Bartic, M.; Toyoda, Y.; Baban, C.-I.; Ogita, M. Oxygen sensitivity in gallium oxide thin films and single crystals at high temperatures. *Jpn. J. Appl. Phys.* **2006**, *45*, 5186–5188. [CrossRef]
101. Manandhar, S.; Battu, A.K.; Devaraj, A.; Shutthanandan, V.; Thevuthasan, S.; Ramana, C.V. Rapid response high temperature oxygen sensor based on titanium doped gallium oxide. *Sci. Rep.* **2020**, *10*, 178. [CrossRef]
102. Frank, J.; Fleischer, M.; Meixner, H. Electrical doping of gas-sensitive, semiconducting Ga_2O_3 thin films. *Sens. Actuators B Chem.* **1996**, *34*, 373–377. [CrossRef]
103. Ogita, M.; Saika, N.; Nakanishi, Y.; Hatanaka, Y. Ga_2O_3 thin films for high-temperature gas sensors. *Appl. Surf. Sci.* **1999**, *142*, 188–191. [CrossRef]
104. Juan, Y.M.; Chang, S.-J.; Hsueh, H.T.; Chen, T.C.; Huang, S.W.; Lee, Y.H.; Hsueh, T.J.; Wu, C.L. Self-powered hybrid humidity sensor and dual-band UV photodetector fabricated on back-contact photovoltaic cell. *Sens. Actuators B Chem.* **2015**, *219*, 43–49. [CrossRef]
105. Zhang, Y.; Feng, Z.; Karim, M.R.; Zhao, H. High-temperature low-pressure chemical vapor deposition of β-Ga_2O_3. *J. Vac. Sci. Technol. A* **2020**, *38*, 050806. [CrossRef]
106. Yu, M.-F.; Atashbar, M.Z.; Chen, X. Mechanical and electrical characterization of β-Ga_2O_3 nanostructures for sensing applications. *IEEE Sens. J.* **2005**, *5*, 20–25. [CrossRef]
107. Feng, P.; Xue, X.Y.; Liu, Y.G.; Wan, Q.; Wang, T.H. Achieving fast oxygen response in individual β-Ga_2O_3 nanowires by ultraviolet illumination. *Appl. Phys. Lett.* **2006**, *89*, 112114. [CrossRef]
108. Huang, Y.; Yue, S.; Wang, Z.; Wang, Q.; Shi, C.; Xu, Z.; Bai, X.D.; Tang, C.; Gu, C. Preparation and electrical properties of ultrafine Ga_2O_3 nanowires. *J. Phys. Chem. B* **2006**, *110*, 796–800. [CrossRef] [PubMed]
109. Liu, Z.; Yamazaki, T.; Shen, Y.; Kikuta, T.; Nakatani, N.; Li, Y.X. O_2 and CO sensing of Ga_2O_3 multiple nanowire gas sensors. *Sens. Actuators B Chem.* **2008**, *129*, 666–670. [CrossRef]
110. Arnold, S.P.; Prokes, S.M.; Perkins, F.K.; Zaghloul, M.E. Design and performance of a simple, room-temperature Ga_2O_3 nanowire gas sensor. *Appl. Phys. Lett.* **2009**, *95*, 103102. [CrossRef]
111. Mazeina, L.; Picard, Y.N.; Maximenko, S.I.; Perkins, F.K.; Glaser, E.R.; Twigg, M.E.; Freitas, J.A., Jr.; Prokes, S.M. Growth of Sn-doped β-Ga_2O_3 nanowires and Ga_2O_3-SnO_2 heterostructures for gas sensing applications. *Cryst. Growth Des.* **2009**, *9*, 4471–4479. [CrossRef]
112. Ma, H.L.; Fan, D.W. Influence of oxygen pressure on structural and sensing properties of β-Ga_2O_3 nanomaterial by thermal evaporation. *Chin. Phys. Lett.* **2009**, *26*, 117302. [CrossRef]
113. Cuong, N.D.; Park, Y.W.; Yoon, S.G. Microstructural and electrical properties of Ga_2O_3 nanowires grown at various temperatures by vapor-liquid-solid technique. *Sens. Actuators B Chem.* **2009**, *140*, 240–244. [CrossRef]
114. Mazeina, L.; Perkins, F.K.; Bermudez, V.M.; Arnold, S.P.; Prokes, S.M. Functionalized Ga_2O_3 nanowires as active material in room temperature capacitance-based gas sensors. *Langmuir* **2010**, *26*, 13722–13726. [CrossRef] [PubMed]
115. Mazeina, L.; Bermudez, V.M.; Perkins, F.K.; Arnold, S.P.; Prokes, S.M. Interaction of functionalized Ga_2O_3 NW-based room temperature gas sensors with different hydrocarbons. *Sens. Actuators B Chem.* **2010**, *151*, 114–120. [CrossRef]
116. Ma, H.L.; Fan, D.W.; Niu, X.S. Preparation and NO_2-gas sensing property of individual β-Ga_2O_3 nanobelt. *Chin. Phys. B* **2010**, *19*, 076102. [CrossRef]
117. Jang, Y.-G.; Kim, W.-S.; Kim, D.-H.; Hong, S.-H. Fabrication of Ga_2O_3/SnO_2 core-shell nanowires and their ethanol gas sensing properties. *J. Mater. Res.* **2011**, *26*, 2322–2327. [CrossRef]
118. Nakagomi, S.; Sai, T.; Kokubun, Y. Hydrogen gas sensor with self temperature compensation based on β-Ga_2O_3 thin film. *Sens. Actuators B Chem.* **2013**, *187*, 413–419. [CrossRef]
119. Nakagomi, S.; Yokoyama, K.; Kokubun, Y. Devices based on series-connected Schottky junctions and β-Ga_2O_3/SiC heterojunctions characterized as hydrogen sensors. *J. Sens. Sens. Syst.* **2014**, *3*, 231–239. [CrossRef]

120. Wu, Y.-L.; Luan, Q.; Chang, S.-J.; Jiao, Z.; Weng, W.Y.; Lin, Y.-H.; Hsu, C.L. Highly sensitive β-Ga_2O_3 nanowire isopropyl alcohol sensor. *IEEE Sens. J.* **2014**, *14*, 401–405. [CrossRef]
121. Zhong, W.; Wang, P.W.; Han, X.B.; Yu, D.P. Gas sensor based on Ga_2O_3 nanowires. *J. Chin. Electron Microsc. Soc.* **2014**, *33*, 7–13. [CrossRef]
122. Reiprich, J.; Isaac, N.A.; Schlag, L.; Hopfeld, M.; Ecke, G.; Stauden, T.; Pezoldt, J.; Jacobs, H.O. Corona discharge assisted growth morphology switching of tin-doped gallium oxide for optical gas sensing applications. *Cryst. Growth Des.* **2019**, *19*, 6945–6953. [CrossRef]
123. Krawczyk, M.; Wozniak, P.S.; Szukiewicz, R.; Kuchowicz, M.; Korbutowicz, R.; Teterycz, H. Morphology of Ga_2O_3 nanowires and their sensitivity to volatile organic compounds. *Nanomaterials* **2021**, *11*, 456. [CrossRef] [PubMed]
124. Kim, H.; Jin, C.; An, S.; Lee, C. Fabrication and CO gas-sensing properties of Pt-functionalized Ga_2O_3 nanowires. *Ceram. Int.* **2012**, *38*, 3563–3567. [CrossRef]
125. Park, S.; Kim, H.; Jin, C.; Lee, C. Synthesis, structure, and room-temperature gas sensing of multiple-networked Pd-doped Ga_2O_3 nanowires. *J. Korean Phys. Soc.* **2012**, *60*, 1560–1564. [CrossRef]
126. Jin, C.; Park, S.; Kim, H.; Lee, C. Ultrasensitive multiple networked Ga_2O_3-core/ZnO-shell nanorod gas sensors. *Sens. Actuators B Chem.* **2012**, *161*, 223–228. [CrossRef]
127. Tsai, T.-Y.; Chang, S.-J.; Weng, W.-Y.; Liu, S.; Hsu, C.-L.; Hsueh, H.-T.; Hsueh, T.-J. β-Ga_2O_3 nanowires-based humidity sensors prepared on GaN/sapphire substrate. *IEEE Sens. J.* **2013**, *13*, 4891–4896. [CrossRef]
128. An, S.; Park, S.; Mun, Y.; Lee, C. UV enhanced NO_2 sensing properties of Pt functionalized Ga_2O_3 nanorods. *Bull. Korean Chem. Soc.* **2013**, *34*, 1632–1636. [CrossRef]
129. Park, S.H.; Kim, S.H.; Park, S.Y.; Lee, C. Synthesis and CO gas sensing properties of surface-nitridated Ga_2O_3 nanowires. *RSC Adv.* **2014**, *4*, 63402–63407. [CrossRef]
130. Juan, Y.M.; Chang, S.-J.; Hsueh, H.T.; Wang, S.H.; Weng, W.Y.; Cheng, T.C.; Wu, C.L. Effects of humidity and ultraviolet characteristics on β-Ga_2O_3 nanowire sensor. *RSC Adv.* **2015**, *5*, 84776–84781. [CrossRef]
131. Bui, Q.C.; Largeau, L.; Morassi, M.; Jegenyes, N.; Mauguin, O.; Travers, L.; Lafosse, X.; Dupuis, C.; Harmand, J.-C.; Tchernycheva, M.; et al. GaN/Ga_2O_3 core/shell nanowires growth: Towards high response gas sensors. *Appl. Sci.* **2019**, *9*, 3528. [CrossRef]
132. Abdullah, Q.N.; Ahmed, A.R.; Ali, A.M.; Yam, F.K.; Hassan, Z.; Bououdina, M. Novel SnO_2-coated β-Ga_2O_3 nanostructures for room temperature hydrogen gas sensor. *Int. J. Hydrogen Energy* **2021**, *46*, 7000–7010. [CrossRef]
133. Park, S.; Kim, S.; Sun, G.-J.; Lee, C. Synthesis, structure and ethanol sensing properties of Ga_2O_3-core/WO_3-shell nanostructures. *Thin Solid Films* **2015**, *591*, 341–345. [CrossRef]
134. Sprincean, V.; Caraman, M.; Spataru, T.; Fernandez, F.; Paladi, F. Influence of the air humidity on the electrical conductivity of the β-Ga_2O_3-GaS structure: Air humidity sensor. *Appl. Phys. A* **2022**, *128*, 303. [CrossRef]
135. Girija, K.; Thirumalairajan, S.; Mastelaro, V.R.; Mangalaraj, D. Catalyst free vapor-solid deposition of morphologically different β-Ga_2O_3 nanostructure thin films for selective CO gas sensors at low temperature. *Anal. Methods* **2016**, *8*, 3224–3235. [CrossRef]
136. Almaev, A.V.; Nikolaev, V.I.; Yakovlev, N.N.; Butenko, P.N.; Stepanov, S.I.; Pechnikov, A.I.; Scheglov, M.P.; Chernikov, E.V. Hydrogen sensors based on Pt/α-Ga_2O_3: Sn/Pt structures. *Sens. Actuators B Chem.* **2022**, *364*, 131904. [CrossRef]
137. Yakovlev, N.N.; Nikolaev, V.I.; Stepanov, S.I.; Almaev, A.V.; Pechnikov, A.I.; Chernikov, E.V.; Kushnarev, B.O. Effect of oxygen on the electrical conductivity of Pt-contacted α-Ga_2O_3/ε(κ)-Ga_2O_3 MSM structures on patterned sapphire substrates. *IEEE Sens. J.* **2021**, *21*, 14636–14644. [CrossRef]
138. Krawczyk, M.; Korbutowicz, R.; Szukiewicz, R.; Wozniak, P.S.; Kuchowicz, M.; Teterycz, H. P-type inversion at the surface of β-Ga_2O_3 epitaxial layer modified with Au nanoparticles. *Sensors* **2022**, *22*, 932. [CrossRef]
139. Liu, K.W.; Sakurai, M.; Aono, M. One-step fabrication of β-Ga_2O_3-amorphous-SnO_2 core-shell microribbons and their thermally switchable humidity sensing properties. *J. Mater. Chem.* **2012**, *22*, 12882. [CrossRef]
140. Weng, T.-F.; Ho, M.-S.; Sivakumar, C.; Balraj, B.; Chung, P.-F. VLS growth of pure and Au decorated β-Ga_2O_3 nanowires for room temperature CO gas sensor and resistive memory applications. *Appl. Surf. Sci.* **2020**, *533*, 147476. [CrossRef]
141. Aymerich, E.L.; Gil, G.D.; Moreno, M.; Pellegrino, P.; Rodriguez, A.R. Fabrication, characterization and performance of low power gas sensors based on $(Ga_xIn_{1-x})_2O_3$ nanowires. *Sensors* **2021**, *21*, 3342. [CrossRef]
142. Ge, X.T.; Fang, D.R.; Liu, X.Q. The preparation and gas-sensing properties of Ga_2O_3-NiO complex oxide by sol-gel method. *Acta Phys. Chim. Sin.* **2005**, *21*, 10–15. [CrossRef]
143. Mohammadi, M.R.; Fray, D.J. Semiconductor TiO_2-Ga_2O_3 thin film gas sensors derived from particulate sol-gel route. *Acta Mater.* **2007**, *55*, 4455–4466. [CrossRef]
144. Mohammadi, M.R.; Fray, D.J.; Ghorbani, M. Comparison of single and binary oxide sol-gel gas sensors based on titania. *Solid State Sci.* **2008**, *10*, 884–893. [CrossRef]
145. Hou, Y.; Jayatissa, A.H. Low resistive gallium doped nanocrystalline zinc oxide for gas sensor application via sol-gel process. *Sens. Actuators B Chem.* **2014**, *204*, 310–318. [CrossRef]
146. Trinchi, A.; Galatsis, K.; Wlodarski, W.; Li, Y.X. A Pt/Ga_2O_3-ZnO/SiC Schottky diode-based hydrocarbon gas sensor. *IEEE Sens. J.* **2003**, *3*, 548–553. [CrossRef]
147. Trinchi, A.; Li, Y.X.; Wlodarski, W.; Kaciulis, S.; Pandolfi, L.; Russo, S.P.; Duplessis, J.; Viticoli, S. Investigation of sol-gel prepared Ga-Zn oxide thin films for oxygen gas sensing. *Sens. Actuators A Phys.* **2003**, *108*, 263–270. [CrossRef]

148. Li, Y.X.; Trinchi, A.; Wlodarski, W.; Galatsis, K.; Kalantar-zadeh, K. Investigation of the oxygen gas sensing performance of Ga_2O_3 thin films with different dopants. *Sens. Actuators B Chem.* **2003**, *93*, 431–434. [CrossRef]
149. Trinchi, A.; Kaciulis, S.; Pandolfi, L.; Ghantasala, M.K.; Li, Y.X.; Wlodarski, W.; Viticoli, S.; Comini, E.; Sberveglieri, G. Characterization of Ga_2O_3 based MRISiC hydrogen gas sensors. *Sens. Actuators B Chem.* **2004**, *103*, 129–135. [CrossRef]
150. Trinchi, A.; Wlodarski, W.; Li, Y.X. Hydrogen sensitive Ga_2O_3 Schottky diode sensor based on SiC. *Sens. Actuators B Chem.* **2004**, *100*, 94–98. [CrossRef]
151. Trinchi, A.; Wlodarski, W.; Faglia, G.; Ponzoni, A.; Comini, E.; Sberveglieri, G. High temperature hydrocarbon sensing with Pt-thin Ga_2O_3-SiC diodes. *Mater. Sci. Forum* **2005**, *483–485*, 1033–1036. [CrossRef]
152. Trinchi, A.; Wlodarski, W.; Li, Y.X.; Faglia, G.; Sberveglieri, G. Pt/Ga_2O_3/SiC MRISiC devices: A study of the hydrogen response. *J. Phys. D Appl. Phys.* **2005**, *38*, 754–763. [CrossRef]
153. Bagheri, M.; Khodadadi, A.A.; Mahjoub, A.R.; Mortazavi, Y. Strong effects of gallia on structure and selective responses of Ga_2O_3-In_2O_3 nanocomposite sensors to either ethanol, CO or CH_4. *Sens. Actuators B Chem.* **2015**, *220*, 590–599. [CrossRef]
154. Lin, H.-J.; Baltrus, J.P.; Gao, H.; Ding, Y.; Nam, C.-Y.; Ohodnicki, P.; Gao, P.-X. Perovskite nanoparticle-sensitized Ga_2O_3 nanorod arrays for CO detection at high temperature. *ACS Appl. Mater. Interfaces* **2016**, *8*, 8880–8887. [CrossRef] [PubMed]
155. Lin, H.-J.; Gao, H.; Gao, P.-X. UV-enhanced CO sensing using Ga_2O_3-based nanorod arrays at elevated temperature. *Appl. Phys. Lett.* **2017**, *110*, 043101. [CrossRef]
156. Chen, H.; Hu, J.B.; Li, G.-D.; Gao, Q.; Wei, C.D.; Zou, X.X. Porous Ga-In bimetallic oxide nanofibers with controllable structures for ultrasensitive and selective detection of formaldehyde. *ACS Appl. Mater. Interfaces* **2017**, *9*, 4692–4700. [CrossRef]
157. Zhang, Y.L.; Jia, C.W.; Kong, Q.; Fan, N.Y.; Chen, G.; Guan, H.T.; Dong, C.J. ZnO-decorated In/Ga oxide nanotubes derived from bimetallic In/Ga MOFs for fast acetone detection with high sensitivity and selectivity. *ACS Appl. Mater. Interfaces* **2020**, *12*, 26161. [CrossRef]
158. Pilliadugula, R.; Krishnan, N. Gas sensing performance of GaOOH and β-Ga_2O_3 synthesized by hydrothermal method: A comparison. *Mater. Res. Express* **2018**, *6*, 025027. [CrossRef]
159. Pilliadugula, R.; Krishnan, N.G. Effect of pH dependent morphology on room temperature NH_3 sensing performances of β-Ga_2O_3. *Mater. Sci. Semicond. Process.* **2020**, *112*, 105007. [CrossRef]
160. Wang, J.; Jiang, S.S.; Liu, H.L.; Wang, S.H.; Pan, Q.J.; Yin, Y.D.; Zhang, G. P-type gas-sensing behavior of Ga_2O_3/Al_2O_3 nanocomposite with high sensitivity to NO_x at room temperature. *J. Alloys Compd.* **2020**, *814*, 152284. [CrossRef]
161. Zhang, B.; Lin, H.-J.; Gao, H.Y.; Lu, X.X.; Nam, C.-Y.; Gao, P.-X. Perovskite-sensitized β-Ga_2O_3 nanorod arrays for highly selective and sensitive NO_2 detection at high temperature. *J. Mater. Chem. A* **2020**, *8*, 10845–10854. [CrossRef]
162. Pilliadugula, R.; Gopalakrishnan, N. Room temperature ammonia sensing performances of pure and Sn doped β-Ga_2O_3. *Mater. Sci. Semicond. Process.* **2021**, *135*, 106086. [CrossRef]
163. Demin, I.E.; Kozlov, A.G. In_2O_3-Ga_2O_3 thin films for ammonia sensors of petrochemical industry safety systems. *AIP Conf. Proc.* **2018**, *2007*, 050004. [CrossRef]
164. Demin, I.E.; Kozlov, A.G. Selectivity of the gas sensor based on the 50% In_2O_3-50% Ga_2O_3 thin film in dynamic mode of operation. *J. Phys. Conf. Ser.* **2018**, *944*, 012027. [CrossRef]
165. Demin, I.E. Increasing the selectivity of semiconductor gas sensors working at sinusoidal-varying temperature for machine industry safety systems. *J. Phys. Conf. Ser.* **2019**, *1260*, 032008. [CrossRef]
166. Demin, I.E. Selection of methods for increasing gas selectivity on the example of a sensor system based on In_2O_3-Ga_2O_3 semiconductor films. *J. Phys. Conf. Ser.* **2019**, *1210*, 012032. [CrossRef]
167. Demin, I.E. Reducing the energy consumption of semiconductor methane sensors for gas alarm systems. *AIP Conf. Proc.* **2019**, *2141*, 050020. [CrossRef]
168. Wei, Z.H.; Akbari, M.K.; Hai, Z.Y.; Ramachandran, R.K.; Detavernier, C.; Verpoort, F.; Kats, E.; Xu, H.Y.; Hu, J.; Zhuiykov, S. Ultra-thin sub-10 nm Ga_2O_3-WO_3 heterostructures developed by atomic layer deposition for sensitive and selective C_2H_5OH detection on ppm level. *Sens. Actuators B Chem.* **2019**, *287*, 147–156. [CrossRef]
169. Jochum, W.; Penner, S.; Fottinger, K.; Kramer, R.; Rupprechter, G.; Klotzer, B. Hydrogen on polycrystalline β-Ga_2O_3: Surface chemisorption, defect formation, and reactivity. *J. Catal.* **2008**, *256*, 268–277. [CrossRef]
170. Vorobyeva, N.; Rumyantseva, M.; Platonov, V.; Filatova, D.; Chizhov, A.; Marikutsa, A.; Bozhev, I.; Gaskov, A. Ga_2O_3 (Sn) oxides for high-temperature gas sensors. *Nanomaterials* **2021**, *11*, 2938. [CrossRef]
171. Pandeeswari, R.; Jeyaprakash, B.G. High sensing response of β-Ga_2O_3 thin film towards ammonia vapours: Influencing factors at room temperature. *Sens. Actuators B Chem.* **2014**, *195*, 206–214. [CrossRef]
172. Yan, J.-T.; Lee, C.-T. Improved detection sensitivity of Pt/β-Ga_2O_3/GaN hydrogen sensor diode. *Sens. Actuators B Chem.* **2009**, *143*, 192–197. [CrossRef]
173. Lee, C.-T.; Yan, J.-T. Investigation of a metal-insulator-semiconductor Pt/mixed Al_2O_3 and Ga_2O_3 insulator/AlGaN hydrogen sensor. *J. Electrochem. Soc.* **2010**, *157*, J281. [CrossRef]
174. Lee, C.-T.; Yan, J.-T. Sensing mechanisms of Pt/β-Ga_2O_3/GaN hydrogen sensor diodes. *Sens. Actuators B Chem.* **2010**, *147*, 723–729. [CrossRef]
175. Shafiei, M.; Hoshyargar, F.; Motta, N.; O'Mullane, A.P. Utilizing p-type native oxide on liquid metal microdroplets for low temperature gas sensing. *Mater. Des.* **2017**, *122*, 288–295. [CrossRef]

176. Saidi, S.A.; Tang, J.; Yang, J.; Han, J.; Daeneke, T.; O'Mullane, A.P.; Kalantar-Zadeh, K. Liquid metal-based route for synthesizing and tuning gas-sensing elements. *ACS Sens.* **2020**, *5*, 1177–1189. [CrossRef]
177. Sivasankaran, B.R.; Balaji, M. Novel gallium oxide/reduced graphene oxide nanocomposite for ammonia gas sensing application. *Mater. Lett.* **2021**, *288*, 129386. [CrossRef]
178. Ji, H.; Zeng, W.; Li, Y. Gas sensing mechanisms of metal oxide semiconductors: A focus review. *Nanoscale* **2019**, *11*, 22664–22684. [CrossRef]
179. Fleischer, M.; Meixner, H. Fast gas sensors based on metal oxides which are stable at high temperatures. *Sens. Actuators B Chem.* **1997**, *43*, 1–10. [CrossRef]
180. Fleischer, M.; Meixner, H. Thin-film gas sensors based on high-temperature-operated metal oxides. *J. Vac. Sci. Technol. A* **1999**, *17*, 1866–1872. [CrossRef]
181. Hoefer, U.; Frank, J.; Fleischer, M. High temperature Ga_2O_3-gas sensors and SnO_2-gas sensors: A comparison. *Sens. Actuators B Chem.* **2001**, *78*, 6–11. [CrossRef]
182. Fleischer, M. Advances in application potential of adsorptive-type solid state gas sensors: High-temperature semiconducting oxides and ambient temperature GasFET devices. *Meas. Sci. Technol.* **2008**, *19*, 042001. [CrossRef]
183. Pohle, R.; Weisbrod, E.; Hedler, H. Enhancement of MEMS-based Ga_2O_3 gas sensors by surface modifications. *Proc. Eng.* **2016**, *168*, 211–215. [CrossRef]
184. Weisz, P.B.; Prater, C.D. Interpretation of measurements in experimental catalysis. *Adv. Catal.* **1954**, *6*, 143. [CrossRef]
185. Jaaniso, R.; Tan, O.K. *Semiconductor Gas Sensors*; Woodhead Publishing: Duxford, UK, 2019; pp. 27–34. [CrossRef]
186. Yamazoe, N. New approaches for improving semiconductor gas sensors. *Sens. Actuators B Chem.* **1991**, *5*, 7–19. [CrossRef]
187. Korotcenkov, G. *Handbook of Gas Sensor Materials*; Springer: New York, NY, USA, 2013; pp. 49–116. [CrossRef]
188. Frank, J.; Fleischer, M.; Meixner, H. Gas-sensitive electrical properties of pure and doped semiconducting Ga_2O_3 thick films. *Sens. Actuators B Chem.* **1998**, *48*, 318–321. [CrossRef]
189. Frank, J.; Fleischer, M.; Meixner, H.; Feltz, A. Enhancement of sensitivity and conductivity of semiconducting Ga_2O_3 gas sensors by doping with SnO_2. *Sens. Actuators B Chem.* **1998**, *49*, 110–114. [CrossRef]
190. Schwebel, T.; Fleischer, M.; Meixner, H. A selective, temperature compensated O_2 sensor based on Ga_2O_3 thin films. *Sens. Actuators B Chem.* **2000**, *65*, 176–180. [CrossRef]
191. Fleischer, M.; Meixner, H. Sensing reducing gases at high temperatures using long-term stable Ga_2O_3 thin films. *Sens. Actuators B Chem.* **1992**, *6*, 257–261. [CrossRef]
192. Hacker, B.; Fleischer, M.; Meixner, H. Topography and performance of gas-sensing devices: An AFM study. *Scanning* **1993**, *15*, 291–294. [CrossRef]
193. Weh, T.; Fleischer, M.; Meixner, H. Optimization of physical filtering for selective high temperature H_2 sensors. *Sens. Actuators B Chem.* **2000**, *68*, 146–150. [CrossRef]
194. Weh, T.; Frank, J.; Fleischer, M.; Meixner, H. On the mechanism of hydrogen sensing with SiO_2 modificated high temperature Ga_2O_3 sensors. *Sens. Actuators B Chem.* **2001**, *78*, 202–207. [CrossRef]
195. Wiesner, K.; Knozinger, H.; Fleischer, M.; Meixner, H. Working mechanism of an ethanol filter for selective high-temperature methane gas sensors. *IEEE Sens. J.* **2002**, *2*, 354–359. [CrossRef]
196. Biskupski, D.; Geupel, A.; Wiesner, K.; Fleischer, M.; Moos, R. Platform for a hydrocarbon exhaust gas sensor utilizing a pumping cell and a conductometric sensor. *Sensors* **2009**, *9*, 7498–7508. [CrossRef] [PubMed]
197. Giber, J.; Perczel, I.V.; Gerblinger, J.; Lampe, U.; Fleischer, M. Coadsorption and cross sensitivity on high temperature semiconducting metal oxides: Water effect on the coadsorption process. *Sens. Actuators B Chem.* **1994**, *18–19*, 113–118. [CrossRef]
198. Reti, F.; Fleischer, M.; Meixner, H.; Giber, J. Effect of coadsorption of reducing gases on the conductivity of β-Ga_2O_3 thin films in the presence of O_2. *Sens. Actuators B Chem.* **1995**, *18–19*, 573–577. [CrossRef]
199. Reti, F.; Fleischer, M.; Meixner, H.; Giber, J. Influence of water on the coadsorption of oxidizing and reducing gases on the β-Ga_2O_3 surface. *Sens. Actuators B Chem.* **1994**, *18*, 138–142. [CrossRef]
200. Reti, F.; Fleischer, M.; Gerblinger, J.; Lampe, U.; Varhegyi, E.B.; Perczel, V.; Meixner, H.; Giber, J. Comparison of the water effect on the resistance of different semiconducting metal oxides. *Sens. Actuators B Chem.* **1995**, *26–27*, 103–107. [CrossRef]
201. Pohle, R.; Fleischer, M.; Meixner, H. In situ infrared emission spectroscopic study of the adsorption of H_2O and hydrogen-containing gases on Ga_2O_3 gas sensors. *Sens. Actuators B Chem.* **2000**, *68*, 151–156. [CrossRef]
202. Varhegyi, E.B.; Perczel, I.V.; Gerblinger, J.; Fleischer, M.; Meixner, H.; Giber, J. Auger and SIMS study of segregation and corrosion some semiconducting oxide gas-sensor materials. *Sens. Actuators B Chem.* **1994**, *18–19*, 569–572. [CrossRef]
203. Hovhannisyan, R.V.; Khondkaryan, H.D.; Aleksanyan, M.S.; Arakelyan, V.M.; Semerjyan, B.O.; Gasparyan, F.V.; Aroutiounian, V.M. Static and noise characteristics of nanocomposite gas sensors. *J. Contemp. Phys.* **2014**, *49*, 151–157. [CrossRef]
204. Dyndal, K.; Zarzycki, A.; Andrysiewicz, W.; Grochala, D.; Marszalek, K.; Rydosz, A. CuO-Ga_2O_3 thin films as a gas-sensitive material for acetone detection. *Sensors* **2020**, *20*, 3142. [CrossRef]
205. Lundstrom, I.; Shivaraman, S.; Svensson, C.; Lundkvist, L. A hydrogen-sensitive MOS field-effect transistor. *Appl. Phys. Lett.* **1975**, *26*, 55–57. [CrossRef]
206. Leu, M.; Doll, T.; Flietner, B.; Lechner, J.; Eisele, I. Evaluation of gas mixtures with different sensitive layers incorporated in hybrid FET structures. *Sens. Actuators B Chem.* **1994**, *18–19*, 678–681. [CrossRef]

207. Geistlinger, H. Accumulation layer model for Ga_2O_3 thin-film gas sensors based on the Volkenstein theory of catalysis. *Sens. Actuators B Chem.* **1994**, *18*, 125–131. [CrossRef]
208. Geistlinger, H.; Eisele, I.; Flietner, B.; Winter, R. Dipole- and charge transfer contributions to the work function change of semiconducting thin films: Experiment and theory. *Sens. Actuators B Chem.* **1996**, *34*, 499–505. [CrossRef]
209. Shin, W.; Hong, S.; Jeong, Y.; Jung, G.; Park, J.; Kim, D.; Park, B.-G.; Lee, J.-H. Effects of channel length scaling on the signal-to-noise ratio in FET-type gas sensor with horizontal floating-gate. *IEEE Electron Device Lett.* **2022**, *43*, 442–445. [CrossRef]
210. Imanaka, N.; Tamura, S.; Adachi, G. Ammonia sensor based on ionically exchanged NH^{4+}-gallate solid electrolytes. *Electrochem. Solid State Lett.* **1999**, *1*, 282. [CrossRef]
211. Westphal, D.; Jakobs, S.; Guth, U. Gold-composite electrodes for hydrocarbon sensors based on YSZ solid electrolyte. *Ionics* **2001**, *7*, 182–186. [CrossRef]
212. Zosel, J.; Westphal, D.; Jakobs, S.; Muller, R.; Guth, U. Au-oxide composites as HC-sensitive electrode material for mixed potential gas sensors. *Solid State Ion.* **2002**, *152–153*, 525. [CrossRef]
213. Zosel, J.; Ahlborn, K.; Muller, R.; Westphal, D.; Vashook, V.; Guth, U. Selectivity of HC-sensitive electrode materials for mixed potential gas sensors. *Solid State Ion.* **2002**, *169*, 115–119. [CrossRef]
214. Zhang, W.-F.; Schmidt-Zhang, P.; Guth, U. Electrochemical studies on cells M/YSZ/Pt (M = Pt, Pt-Ga_2O_3) in NO, O_2, N_2 gas mixtures. *Solid State Ion.* **2004**, *169*, 121–128. [CrossRef]
215. Shuk, P.; Bailey, E.; Zosel, J.; Guth, U. New advanced in situ carbon monoxide sensor for the process application. *Ionics* **2009**, *15*, 131–138. [CrossRef]
216. Wu, N.Q.; Chen, Z.; Xu, J.H.; Chyu, M.; Mao, S.X. Impedance-metric Pt/YSZ/Au-Ga_2O_3 sensor for CO detection at high temperature. *Sens. Actuators B Chem.* **2005**, *110*, 49–53. [CrossRef]
217. Yan, S.C.; Wan, L.J.; Li, Z.S.; Zhou, Y.; Zou, Z.G. Synthesis of a mesoporous single crystal Ga_2O_3 nanoplate with improved photoluminescence and high sensitivity in detecting CO. *Chem. Commun.* **2010**, *46*, 6388. [CrossRef]
218. Korotcenkov, G.; Han, S.H.; Cho, B.K. Material design for metal oxide chemiresistive gas sensors. *J. Sens. Sci. Technol.* **2013**, *22*, 1–17. [CrossRef]
219. Bartic, M.; Ogita, M.; Isai, M.; Baban, C.; Suzuki, H. Oxygen sensing properties at high temperatures of β-Ga_2O_3 thin films deposited by the chemical solution deposition method. *J. Appl. Phys.* **2007**, *102*, 023709. [CrossRef]
220. Wang, D.; Lou, Y.L.; Wang, R.; Wang, P.P.; Zheng, X.J.; Zhang, Y.; Jiang, N. Humidity sensor based on Ga_2O_3 nanorods doped with Na^+ and K^+ from GaN powder. *Ceram. Int.* **2015**, *41*, 14790–14797. [CrossRef]
221. Potje-Kamloth, K. Semiconductor junction gas sensors. *Chem. Rev.* **2008**, *108*, 367–399. [CrossRef]
222. Ratko, A.; Babushkin, O.; Baran, A.; Baran, S. Sorption and gas sensitive properties of In_2O_3 based ceramics doped with Ga_2O_3. *J. Eur. Ceram. Soc.* **1998**, *18*, 2227–2232. [CrossRef]
223. Silver, A.T.; Juarez, A.S. SnO_2: Ga thin films as oxygen gas sensor. *Mater. Sci. Eng. B* **2004**, *110*, 268–271. [CrossRef]
224. Bagheri, M.; Khodadadi, A.A.; Mahjoub, A.R.; Mortazavi, Y. Highly sensitive gallia-SnO_2 nanocomposite sensors to CO and ethanol in presence of methane. *Sens. Actuators B Chem.* **2013**, *188*, 45–52. [CrossRef]
225. Du, L.T.; Li, H.Y.; Li, S.; Liu, L.; Li, Y.; Xu, S.Y.; Gong, Y.M.; Cheng, Y.L.; Zeng, X.G.; Liang, Q.C. A gas sensor based on Ga-doped SnO_2 porous microflowers for detecting formaldehyde at low temperature. *Chem. Phys. Lett.* **2018**, *713*, 235–241. [CrossRef]
226. Kevin, M.; Tho, W.H.; Ho, G.W. Transferability of solution processed epitaxial Ga:ZnO films; tailored for gas sensor and transparent conducting oxide applications. *J. Mater. Chem.* **2012**, *22*, 16442. [CrossRef]
227. Vorobyeva, N.; Rumyantseva, M.; Filatova, D.; Konstantinova, E.; Grishina, D.; Abakumov, A.; Turner, S.; Gaskov, A. Nanocrystalline ZnO(Ga): Paramagnetic centers, surface acidity and gas sensor properties. *Sens. Actuators B Chem.* **2013**, *182*, 555–564. [CrossRef]
228. Rashid, T.-R.; Phan, D.-T.; Chung, G.-S. Effect of Ga-modified layer on flexible hydrogen sensor using ZnO nanorods decorated by Pd catalysts. *Sens. Actuators B Chem.* **2014**, *193*, 869–876. [CrossRef]
229. Girija, K.G.; Somasundaram, K.; Debnath, A.K.; Topkar, A.; Vatsa, R.K. Enhanced H_2S sensing properties of gallium doped ZnO nanocrystalline films as investigated by DC conductivity and impedance spectroscopy. *Mater. Chem. Phys.* **2018**, *214*, 297–305. [CrossRef]
230. Fleischer, M.; Meixner, H. Selectivity in high-temperature operated semiconductor gas-sensors. *Sens. Actuators B Chem.* **1998**, *52*, 179–187. [CrossRef]
231. Anichini, C.; Czepa, W.; Pakulski, D.; Aliprandi, A.; Ciesielski, A.; Samori, P. Chemical sensing with 2D materials. *Chem. Soc. Rev.* **2018**, *47*, 4860–4908. [CrossRef]
232. Zhao, J.L.; Huang, X.R.; Yin, Y.H.; Liao, Y.K.; Mo, H.W.; Qian, Q.K.; Guo, Y.Z.; Chen, X.L.; Zhang, Z.F.; Hua, M.Y. Two-dimensional gallium oxide monolayer for gas-sensing application. *J. Phys. Chem. Lett.* **2021**, *12*, 5813–5820. [CrossRef]
233. Wang, S.; Li, H.; Huang, H.; Cao, X.; Chen, X.; Cao, D. Porous organic polymers as a platform for sensing applications. *Chem. Soc. Rev.* **2022**, *51*, 2031–2080. [CrossRef]
234. Yang, Y.; Zhang, P. Dissociation of H_2 molecule on the β-Ga_2O_3 (100)B surface: The critical role of oxygen vacancy. *Phys. Lett. A* **2010**, *374*, 4169–4173. [CrossRef]
235. Nagarajan, V.; Chandiramouli, R. Methane adsorption characteristics on β-Ga_2O_3 nanostructures: DFT investigation. *Appl. Surf. Sci.* **2015**, *344*, 65–78. [CrossRef]

236. Yaqoob, U.; Younis, M.I. Chemical gas Sensors: Recent developments, challenges, and the potential of machine Learning—A review. *Sensors* **2021**, *21*, 2877. [CrossRef] [PubMed]
237. Mohmed, M.; Attia, N.; Elashery, S. Greener and facile synthesis of hybrid nanocomposite for ultrasensitive iron (II) detection using carbon sensor. *Microporous Mesoporous Mater.* **2021**, *313*, 110832. [CrossRef]
238. Elashery, S.; Attia, N.; Oh, H. Design and fabrication of novel flexible sensor based on 2D Ni-MOF nanosheets as a preliminary step toward wearable sensor for onsite Ni (II) ions detection in biological and environmental samples. *Anal. Chim. Acta* **2022**, *1197*, 339518. [CrossRef] [PubMed]
239. Rahman, T.; Masui, T.; Ichiki, T. Single-crystal gallium oxide-based biomolecular modified diode for nucleic acid sensing. *Jpn. J. Appl. Phys.* **2015**, *54*, 04DL08. [CrossRef]
240. Das, M.; Chakraborty, T.; Lin, C.H.; Lin, R.; Kao, C.H. Screen-printed Ga_2O_3 thin film derived from liquid metal employed in highly sensitive pH and non-enzymatic glucose recognition. *Mater. Chem. Phys.* **2022**, *278*, 125652. [CrossRef]